Modeling *Braf*-induced thyroid cancer development and drug screening using pluripotent stem cell-derived organoids

Hélène Lasolle [1], Andrea Schiavo [1], Adrien Tourneur[1], Pierre Gillotay [1], Bárbara de Faria da Fonseca [1], Lucieli Ceolin [1, 6], Olivier Monestier [1], Benilda Aganahi [1], Laura Chomette [1], Marina Malta Letro Kizys [1], Lieven Haenebalcke [2], Tim Pieters [2, 3], Steven Goossens [2, 4], Jody Haigh [2, 5], Vincent Detours [1], Ana Luiza Silva Maia [6], Sabine Costagliola [1] and Mírian Romitti [1*]

[1] Institut de Recherche Interdisciplinaire en Biologie Humaine et Moléculaire (IRIBHM), Université Libre de Bruxelles (ULB), Brussels, Belgium

[2] VIB, Flanders Institute for Biotechnology, Ghent University, Ghent, Belgium

[3] Department of Biomolecular Medicine, Faculty of Medicine and Health Sciences, Ghent University, Ghent, Belgium

[4] Department of Diagnostic Sciences, Faculty of Medicine and Health Sciences, Ghent University, Ghent, Belgium

[5] CancerCare Manitoba Research Institute, Department of Pharmacology and Therapeutics, Rady Faculty of Health Sciences, University of Manitoba, Winnipeg, Manitoba, Canada

[6] Thyroid Section, Endocrine Division, Hospital de Clínicas de Porto Alegre (HCPA), Universidade Federal do Rio Grande do Sul (UFRGS), Porto Alegre, Brazil

* Corresponding author: mirian.romitti@ulb.be

Abstract

Thyroid cancer is the most common endocrine malignancy and several genetic events have been described to promote the development of thyroid carcinogenesis. Besides the effects of specific mutations on thyroid cancer development, the molecular mechanisms controlling tumorigenesis, tumor behavior, and drug resistance are still largely unknown. Cancer organoids have been proposed as a powerful tool to study aspects related to tumor development and progression and appear promising to test individual responses to therapies. Here, using mESC-derived thyroid organoids, we developed a Braf^{V637E}-inducible model able to recapitulate the features of papillary thyroid cancer in vitro. Overexpression of Braf^{V637E} rapidly leads to MAPK activation, cell dedifferentiation, and disruption of follicular organization. Braf^{V637E}-expressing organoids show a transcriptomic signature for p53, focal adhesion, ECM-receptor interactions, EMT, and inflammatory signaling pathways. Finally, PTC-like thyroid organoids were used for drug screening assays. The combination of MAPK and PI3K inhibitors reversed *Braf* oncogene-promoted cell dedifferentiation while restoring thyroid follicle organization and function *in vitro*. Our results demonstrate that pluripotent stem cells-derived thyroid cancer organoids can mimic tumor development and features while providing an efficient tool for testing novel targeted therapies.

Introduction

Pluripotent Stem Cells (PSCs) emerged as a model to dissect and recapitulate the molecular events and gene networks that regulate cell fate determination, cell differentiation and organogenesis. Guided differentiation of PSCs into 3D organized tissue by inducible overexpression of specific transcription or growth factors and inhibitors allows the derivation of *in vitro* organoids and the understanding of

51 mechanisms regulating cell differentiation and tissue formation[1]. Due to their remarkable
52 self-organizing structures and functional properties, organoids technology became a
53 powerful tool to model organ development and disease 'in a dish' [2,3].

54 In the last decade, the use of organoids for cancer research emerged and opened
55 new possibilities to better understand tumor behavior. Initially, colon, prostate,
56 pancreatic, ovarian, lung and thyroid cancer-derived organoids have been efficiently
57 generated, which resemble phenotypically and genetically the tumor of origin[4–13].
58 Currently, a large set of healthy and tumour matching organoids has been generated and
59 is available through biobanks. These patient-derived organoids are particularly interesting
60 in testing individual responses to therapies[8,13,14].

61 Recently, studies have reported the generation of cancer models arising from
62 healthy (adult stem cells or aSCs and PSCs) organoids by controlling oncogene
63 expression[15–17]. By using gene expression manipulation tools, such as shRNA and
64 CRISPR-Cas9, murine stomach cancer (Cdh1$^{-/-}$; Tp53$^{-/-}$)[18], murine and human colon
65 cancer (APC, TP53, KRAS and Smad4 mutations)[15,16,19], human pancreatic cancer
66 (KRAS and/or TP53 mutations)[4,20] and human lung adenocarcinoma organoids (HER2
67 overexpression) could be efficiently generated[17]. Compared to patient-derived organoids,
68 healthy stem cells-derived cancer organoids are suitable to address additional questions
69 such as precise effects of oncogenes and early events driving tumorigenesis; the role of
70 cancer stem cells on tumor induction, genomic stability, the effect of treatments at
71 different stages of carcinogenesis and screening for new therapeutical tools[21]. Besides,
72 they allow multiple reproducible experiments free from inter-individual variability.

73 Thyroid cancer is the most frequent endocrine malignancy, and several genetic
74 events have been described as driving thyroid carcinogenesis. Papillary thyroid
75 carcinoma (PTC) is the most common malignant thyroid tumor[22], and aberrant activation

76 of the MAPK pathway is a hallmark[23]. The BRAF^{V600E} mutation is the most frequent
77 genetic event, accounting for around 50% of PTCs[24–26] and results is an oncogenic protein
78 with markedly elevated kinase activity that constitutively induces MEK/ERK signaling
79 transduction[27–29].

80 BRAF-mutated thyroid tumors are often less differentiated, mainly due to the
81 lower expression levels of thyroid functional genes *NIS, TSHR, TG* or *TPO,* leading to a
82 low Thyroid Differentiation Score (TDS)[30]. This dedifferentiated state is associated with
83 a worse clinical condition and with a higher rate of radioactive iodine (RAI) refractory
84 tumors[31,32]. However, its impact on prognosis is still uncertain, as BRAF^{V600E} alone has
85 not been proven to be an independent prognostic factor[33,34]. On the other hand, *BRAF* and
86 *TERT* promoter mutated tumors have been associated with higher specific mortality[35].
87 Also, studies have shown a small proportion (around 20%) of BRAF^{V600E} mutated tumors
88 presenting a higher level of differentiation associated with a less aggressive behavior and
89 a preserved RAI uptake ability[30,36]. This suggests a possible cell heterogeneity among the
90 BRAF^{V600E} mutated tumors.

91 Some years ago, our group showed the generation of functional 3D thyroid tissue
92 derived from mouse embryonic stem cells (mESC)[37] and, recently human thyroid
93 organoids were generated using the same approach[38]. The differentiation protocol relies
94 on transient induction of *Nkx2.1* and *Pax8* thyroid transcription factors allowing an
95 efficient generation of thyroid follicular cells organized into three-dimensional follicular
96 structures capable of thyroid hormone production *in vitro* and *in vivo*. This model and
97 further developed thyroid organoids from healthy mouse and human PSCs/aSC[39–49] open
98 new perspectives to explore thyroid development processes and to model thyroid
99 diseases, including thyroid cancer.

100 So far, efficient, fast and cost-effective tools are lacking to functionally

101 characterize a large set of candidate genes in the context of thyroid carcinogenesis.
102 Thyroid cancer organoids/spheroids models have been recently described based on
103 patient tumor-derived models[50–54]. Patient-derived organoid might be used to study
104 patient-specific tumor behavior and the treatment response on a case-to-case basis. It is
105 patient-to-patient dependent with high heterogeneity and low reproducibility. It is limited
106 by the accessibility to samples and since it is derived from an already established tumor,
107 it is not suitable to study mechanisms related to cancer development and drugs resistance
108 acquisition. Saito et al. described a mouse model of poorly differentiated thyroid
109 carcinoma obtained after transplantation of thyroid organoids derived from Tp53
110 knockout mice with NRAS activating mutation overexpression[12]. Recently, Veschi *et al.*
111 [55] generated of PTC and FTC organoids models by inducing *BRAF*, *NRAS* and *TP53*
112 mutations in thyroid progenitors derived from hESC. After transplantation, the tumors
113 generated resemble Papillary and Follicular tumors and, transcriptomics analysis
114 suggested a role of Kisspeptin receptor (KISS1R) in cooperation with Tissue Inhibitor of
115 Metalloproteinase 1 (TIMP1)/Matrix metallopeptidase 9 (MMP9)/Cluster of
116 differentiation 44 (CD44), on tumor development and progression[55].
117 Here, we aim to develop an *in vitro* PTC organoid model to screen for targets and
118 drugs by taking advantage of our model of thyroid generation by includible expression of
119 $Braf^{V637E}$ mutation in mouse ESC-derived functional thyroid follicles.
120
121 **Methods**
122
123 *Cell culture and mESC_$Braf^{V637E}$ line generation*

124 The previously genetically modified G4 RosaLuc mouse embryonic stem cell line
125 (mESC)[56] was initially cultured on gamma-irradiated mouse embryonic fibroblasts

126 (MEFs) feeder using mouse stem cell medium[37,57] and incubated at 37 °C, 5 % CO^2 and
127 >95 % humidity. To insert the target sequences into the modified Rosa26 locus of G4
128 RosaLuc mESCs, around $1x10^5$ cells were transfected using the Flpe expressing vector[56]
129 and the target vector containing the rtTA-TRE induction system, thyroid transcription
130 factors, Nkx2-1 and Pax8 and bTg-NES-$Braf^{V637E}$-ERT^2 sequences (Figure S1A)
131 following the lipofectamine 3000 protocol (Thermo Scientific). The $Braf^{V637E}$ mutation
132 here used for mouse cells is equivalent to the human $BRAF^{V600E}$ mutation[58]. G418 (300
133 µg/ml) was applied 48 h after transfection, typically for 10 days, and individual clones
134 were picked and further expanded. Clones were screened for by immunofluorescence for
135 Nkx2-1 and Pax8 expression induction after three days of incubation with 1 µg/ml
136 Doxycyclin (Dox) (Figure S1B). Positive clones were then characterized according to
137 pluripotency maintenance (Figure S1C), *Nkx2-1* and *Pax8* expression, and efficiency of
138 thyroid differentiation. In addition, we generated an mESC control line where the
139 sequences of NES-$BRAF^{V637E}$-ERT^2 were replaced by the eGFP sequence, resulting in
140 the TRE-Nkx2-1-Pax8_bTg-eGFP line (Figure S1D). The mESC control line generation,
141 selection and characterization were performed as described above (Figures S1E and F).

142 *Thyroid differentiation protocol*

143 G4 RosaLuc TRE-Nkx2-1-Pax8_bTg-NES-$Braf^{V637E}$-ERT^2 and TRE-Nkx2-1-
144 Pax8_bTg-eGFP cells were cultured and differentiated as described previously by
145 Antonica *et al.* (2012)[37] with few modifications. Briefly, embryoid bodies (EBs),
146 generated by hanging drops were collected after four days and embedded in growth factor
147 reduced Matrigel (GFR MTG; BD Biosciences); 50µl MTG drops (containing around 20
148 EBs) were plated into 12-wells plates. EBs were differentiated using a differentiation
149 medium initially supplemented with 1µg/ml of Doxycycline (Sigma) for five days,
150 followed by two weeks of maturation induction by using 0.3 µmol of 8-Br-cAMP

151 (BioLog) or 1mU ml^{-1} of thyrotropin (hrTSH; Genzyme). Thyroid differentiation and
152 functionality were evaluated by transcriptomics (RT-PCR and bulk RNA sequencing),
153 immunofluorescence and iodide organification.
154
155 *Braf^{V637E} induction and drug screening*
156 After full thyroid maturation (Day 25), MTG drops were washed twice with Hanks's
157 balanced salt solution (HBSS, containing calcium and magnesium; Invitrogen) and
158 incubated in an HBSS solution (1 ml per well) containing 10 U/ml of dispase II (Roche)
159 and 125 U/ml of collagenase type IV (Sigma) for 30 min at 37°C. Then the enzymes were
160 inactivated by adding 10% FBS and cells were centrifuged at 500g for 3 min. Cells were
161 rinsed twice with HBSS, and the follicles population was enriched by filtering using 30
162 μm (single cell removal) and 100 μm reverse strainer (Pluriselect). Finally, enriched
163 structures were re-embedded in GFR MTG (50μl) and plated into 12-well plates. Twenty-
164 four hours later, cells were incubated with 1 μM of 4-Hydroxytamoxifen (4OHT) (Sigma)
165 and 8-Br-cAMP or hrTSH for 24h, 48h or 7 days to promote Braf^{V637E}-induced
166 phosphorylation of MAPK pathway[58].
167 In addition, Braf-induced thyroid organoids (previously treated for four days with 4OHT)
168 were cultured with distinct compounds, previously suggested to regulate Nis re-
169 expression and inhibit *Braf* oncogenic effects[59,60]. Among the screened drugs, several
170 cell processes were targeted by the following compounds: PD0325901 (MEK inhibitor;
171 250nM; Stem Cell), LY204002 (PI3K inhibitor; 5μM; Selleckchem), VPA (HDAC
172 inhibitor; 250μM; Sigma), NAC (N-acetyl cysteine, antioxidant compound; 2mM;
173 Sigma), 5-AZA-2' deoxycytidine (DNA methyltransferase (DMNT) inhibitor; 1μM;
174 Sigma) and RG108 (DMNT inhibitor; 10μM; Sigma).
175

176 *Flow cytometry - Proliferation analysis*

177 Control condition (4OHT-) and organoids treated with 4OHT for 6 days were treated with
178 BrdU (1mM) for 3 hours, collected and prepared for immunostaining as follows: Matrigel
179 drops (at least five samples per condition) were first digested with HBSS solution
180 containing 10 U/ml dispase II and 125 U/ml collagenase type IV for 30-60 min at 37°C;
181 then a single cell suspension was obtained by dissociation with TripLE Express for 10-
182 15 min incubation at 37°C, the enzymes were inactivated by addition of differentiation
183 medium. After centrifugation, samples were rinsed with PBS, and then the BrdU Flow
184 Kit staining protocol (BD) was used according to the manufacturer's instructions. In order
185 to identify the BrdU incorporated cells among the thyroid population, cells were also
186 stained using primary Nkx2-1 antibody (1:100) and anti-rabbit IgG Alexa fluor 647-
187 conjugated secondary antibody (1:300). Non-stained and only secondary-incubated cells
188 were used as a negative control for gate strategy. LSR-Fortessa X-20 flow cytometer was
189 used for quantification, and FACSDiva software was used for the analysis. Data are
190 presented as a percentage of positive cells.

191

192 *Immunofluorescence staining*

193 Organoids embedded in MTG were fixed in 4% paraformaldehyde (PFA; Sigma) for 1 h
194 at room temperature (RT) and washed three times in PBS. Blocking was performed using
195 a solution of PBS containing 3% bovine serum albumin (BSA; Sigma), 5% horse serum
196 (Invitrogen) and 0.3% Triton X-100 (Sigma) for 30 min at RT. The primary and
197 secondary antibodies were diluted in a solution of PBS containing 3% BSA, 1% horse
198 serum and 0.1% Triton X-100. Primary antibodies were incubated overnight at 4°C
199 followed by incubation with secondary antibodies and Hoechst for 2 h at RT. Slides were
200 mounted with Glycergel (Dako).

201 Organoids were fixed overnight at 4°C in 4% PFA for paraffin embedding and kept in
202 70% ethanol at 4°C before embedding. Samples were then embedded in paraffin,
203 sectioned (5 μm), mounted on glass slides, deparaffinized, and rehydrated. For
204 immunostaining, antigen retrieval was performed by incubating the sections for 10 min
205 in the microwave (850 W) in Sodium Citrate Buffer (10 mM Sodium Citrate, 0.05%
206 Tween 20, pH 6.0). After cooling, the sections were rinsed with PBS and blocked with
207 1% BSA and 10% horse serum PBS solution for 1 h at RT. Primary antibodies were
208 diluted (as described above) in the blocking solution and incubated overnight at 4°C. The
209 sections were rinsed three times in PBS and incubated with Hoechst and secondary
210 antibodies diluted in blocking solution for 1 h at room temperature. Slides were mounted
211 with Glycergel (Dako). Imaging was performed using a Zeiss LSM510 META confocal
212 microscope and a Leica DMI6000 microscope with DFC365FX camera. The antibodies
213 information is listed in the supplementary Table 1.
214
215 *Western blot*
216 Organoids were initially isolated (collagenase IV/dispase II solution, described above)
217 from at least 6 distinct wells and pooled together for protein extraction using RIPA buffer.
218 The protein concentration was determined according to Pierce 660 nm protein assay
219 reagent protocol (Thermo Scientific). Briefly, each sample's 30–50 μg of protein was
220 fractionated by 10% SDS–PAGE and blotted onto an Immobilon PVDF membrane
221 (Millipore). Blocking of non-specific binding sites were blocked by incubation with 5%
222 BSA in Tris-buffered saline (TBS) 0.1% Tween-20 for 1 h. Thereafter, the membrane
223 was incubated overnight at 4 °C with primary antibodies against p-ERK and β-Actin in a
224 blocking solution. Next, the membrane was incubated with horseradish peroxidase-
225 conjugated anti-rabbit or anti-mouse antibody in a blocking solution, for 60 min at RT.

226 The antigen-antibody complexes were visualized using an enhanced chemiluminescence
227 system (GE Healthcare) and captured by Azure 500 system (Azure Biosystems).
228
229 *Iodide organification assay*
230 Thyroid organoids treated with cAMP, cAMP+4OHT, cAMP+4OHT+PD+LY and
231 cAMP+4OHT+PD+LY+VPA were tested for the ability of iodide uptake and
232 organification as previously described[37,57]. Briefly, cells were washed with HBSS and
233 incubated with 1 ml per well of an organification medium containing 1,000,000 c.p.m.
234 per ml ^{125}I (PerkinElmer) and 100 nM sodium iodide (NaI, Sigma) in HBSS for 2 h at 37
235 °C. After, the reaction was stopped by the addition of methimazole (MMI; 4 mM, Sigma).
236 After two cold PBS washes, cells were detached using trypsin/EDTA (Invitrogen). For
237 iodide uptake quantification, cells were collected, and radioactivity was measured using
238 a c-counter. Subsequently, proteins were precipitated by adding 1 mg of gamma-globulins
239 (Sigma) and 20% TCA followed by centrifugation at 2,000 r.p.m. for 10 min, at 4°C and
240 the radioactivity of protein-bound ^{125}I (PBI) was measured. Iodide organification was
241 calculated as an iodide uptake/PBI ratio and, the values were expressed as a percentage.
242 Cells were also treated with 1 mM sodium perchlorate (Nis inhibitor; NaClO4, Sigma-
243 Aldrich) and 2 mM MMI (Tpo inhibitor; Sigma-Aldrich) as iodide uptake and protein-
244 binding controls, respectively. The experiments were performed in triplicates for each
245 condition.
246
247 *Gene expression analysis*
248 Real-time PCR (RT-qPCR) was performed on cDNA from thyroid organoids from at least
249 three independent experiments. Total RNA was extracted from thyroid organoids by the
250 addition of lysis RLT Lysis buffer (Qiagen) + 1% 2-mercaptoethanol directly on the MTG

251 drop containing the organoids. RNA was isolated using the RNeasy micro kit (Qiagen)
252 according to the manufacturer's instructions. cDNA was generated by reverse
253 transcription using the Superscript II kit (Invitrogen). qPCR was performed on cDNA in
254 triplicates using Takyon™ No ROX SYBR 2X MasterMix blue dTTP (Eurogentec) and
255 CFX Connect Real-Time System (Biorad). Results are presented as linearized values
256 normalized to the housekeeping gene, β2-microglobulin and the indicated reference value
257 (2-DDCt). Primer sequences are described in supplementary Table 2.

258 *Bulk RNA sequencing and analysis*

259 Bulk RNA-seq was performed on day 31, using the cAMP, cAMP+4OHT (5 days) and
260 cAMP+4OHT+PD+LY (3 days) conditions (see protocol, Figure 5A). RNA extraction
261 was performed as previously described (section "*Gene expression analysis"*), and
262 experiments were performed in duplicates. At least three distinct wells were pooled
263 together for each condition. RNA quality and concentration were evaluated using
264 Bioanalyser 2100 (Agilent) and RNA 6000 Nano Kit (Agilent). RNA integrity was
265 preserved, and no genomic DNA contamination was detected. Indexed cDNA libraries
266 were obtained using the TruSeq Stranded mRNA Sample Prep kit (Illumina) using an S2
267 flow cell, and sequences were produced using a 200 cycles reagent kit. The resulting high-
268 quality indexed cDNA libraries were quantified with the Quant-iT PicoGreen kit (Life
269 Sciences) and Infinite F200 Proplate reader (Tecan); DNA fragment size distribution was
270 examined with the 2100 Bioanalyzer (Agilent) using the DNA 1000 kit (Agilent).
271 Multiplexed libraries (10ρM) were loaded onto flow cells and sequenced on the HiSeq
272 1500 system (Illumina) in high-output mode using the HiSeq Cluster Kit v4 (Illumina).
273 The sequenced data were uploaded on the galaxy web platform version 22.05.1, and the
274 public server https://usegalaxy.eu was used for mapping and counting analysis.
275 Approximately 10 million paired-end reads were obtained per sample. After the removal

276 of low-quality bases and Illumina adapter sequences using Trimmomatic software[61],
277 paired-end reads were mapped against the mouse reference genome mm10 (GRCm38)
278 using HISAT2 sofware[62], allowing soft clipping. Raw read counts were obtained using
279 HTseq count software with unstranded option[63]. Low-expressed genes were filtered
280 using the EdgeR package in R software (https://www.r-project.org). Then, differential
281 expression analysis was performed using DESeq2 package[64]. Fold change and adjusted
282 p-value thresholds of 2 and 0.05, respectively were used to select differentially expressed
283 genes (DEG). Gene ontology and pathways enrichment analysis in up and down
284 differentially expressed gene lists was realized using EnrichR
285 (https://maayanlab.cloud/Enrichr/). Transformed counts corresponding to log2
286 (normalized counts +4) using the DESeq2 package were used for further analysis and
287 heatmap visualization. Thyroid differentiation score (TDS), Enhanced Thyroid
288 differentiation score (eTDS) and ERK activation score were calculated as previously
289 described[65]. The list of the genes used for the score's calculation is provided in
290 supplementary Table 3.
291
292 *Data availability*
293 The data that support this study are available from the corresponding author upon request.
294 Bulk RNA-seq data have been deposited in the NCBI Gene Expression Omnibus under
295 accession number GSE228281.
296
297 *Statistical analysis*
298 All statistical analysis were performed using GraphPad Prism 9. Comparison between
299 two groups and its statistical significance was tested using the unpaired *t*-test or
300 nonparametric Mann-Whitney U test. In contrast, comparison between multiple groups

301 was performed using one-way ANOVA or nonparametric Kruskal-Wallis test. Data are
302 displayed as mean ± SD or median (IQR). Differences were considered significant at
303 $p<0.05$ and presented as follows: *$p < 0.05$, **$p < 0.01$, ***$p < 0.001$, ****$p < 0.0001$.
304 All the data presented are from at least three independent experiments.
305
306 **Results**
307 *mESC_BRAF^{V637E} cell line generation and characterization*
308 We combined the previously described mESC transient induction thyroid differentiation
309 strategy (Antonica, 2012) with a Braf^{V637E}-ERT^2 inducible model (Ortiz, 2013) to
310 generate a double-inducible recombinant mESC_BRAF^{V637E} cell line. The resulting
311 mESC_Nkx2-1/Pax8_bTg_Braf^{V637E}_ERT^2 clones were initially selected and
312 characterized by the response to doxycycline (Dox) treatment, confirmed by the
313 overexpression of Nkx2-1 and Pax8; and ability to spontaneously differentiate into cells
314 from the three germ-layers (Figures S1A, B and C, respectively). In addition, a control
315 mESC line was generated in which Braf^{V637E}_ERT^2 system was replaced by the eGFP
316 sequence. Similarly, the control line responded properly to Dox induction and maintained
317 the pluripotency capacity (Figures S1D, E and F, respectively).
318
319 *Thyroid differentiation protocol*
320 The capability of the new cell line to generate thyroid follicles and express the Braf^{V637E}
321 oncogene was demonstrated following the mESC thyroid differentiation protocol[37,57,66].
322 Since we used a newly modified mESC line, the steps of the differentiation protocol were
323 tested and adapted accordingly (Figure 1A). Here, using the mESC_Nkx2-
324 1/Pax8_bTg_Braf^{V637E} line, we observed that Dox stimulation for 5 days leads to higher
325 exogenous and endogenous *Nkx2-1*, *Pax8* and *Tg* mRNA (day 9; Figure S2E) compared

326 to 3 or 4 days of treatment (Figure S2A-D). Similar results were obtained using the control
327 mESC line (Figure S2A-D). Next, two weeks of treatment with cAMP (from day 9 to 23)
328 markedly induced the expression levels of *Nkx2-1, Pax8, Tg, TshR, Nis* and *Tpo* when
329 compared to the control (-Dox -cAMP) (Figure 1B). Accordingly, immunofluorescence
330 staining showed follicular organized Nkx2-1 and Tg-expressing cells (Figure 1C), in
331 which the functionality is demonstrated by intraluminal iodinate-Tg (Tg-I) accumulation
332 (Figure 1D). Since our protocol also generates other cell types than thyroid[57], a follicle
333 enrichment step was added to the protocol to enrich the follicular structures and induce
334 Braf-oncogene in a purer population. This protocol led to an increase of thyroid markers
335 levels (Figure 1E) when compared to the non-enriched control condition, while the
336 follicular structure and functionality were preserved as demonstrated by Nkx2-1, Nis and
337 Tg-I staining (Figure 1F-G). Notably, after re-embedding in Matrigel (MTG), follicles
338 could be maintained in culture for at least 28 additional days without major histological
339 changes (data not shown).
340
341 *Braf^{V637E} induction on thyroid organoids leads to PTC-like phenotype*
342 To ensure that Braf^{V637E} oncogene is expressed specifically among follicular thyroid cells,
343 we used the bovine Tg (bTg) as a promoter controlling Braf^{V637E}_ERT^{2} expression.
344 Effectively, exogenous *Braf^{V637E}* mRNA expression was rapidly induced after Dox
345 treatment (Day 9; Figure S2E), maintaining the expression levels stable over time (Figure
346 1B and Figure S3A), while *Tg* mRNA expression increased following the differentiation
347 program (Figure S3A). Even if *Braf^{V637E}* expression is driven by the bTg promoter, the
348 Braf-mutated protein is not active/phosphorylated since it is maintained in the nucleus in
349 an inactive complex with HSP90. The addition of 4OHT induces nuclear translocation of
350 the Braf mutant to the cytoplasm (NES signal), then driving MAPK activation[58] (Figure

351 2A). Indeed, 24 hours after 4OHT addition, we observed an increase in ERK
352 phosphorylation (pERK) compared to the control condition (cAMP), which was
353 maintained after 7 days of continuous 4OHT treatment (Figure 2B). To assess Braf-
354 induced cell proliferation, flow cytometry analysis performed after 6 days of 4OHT
355 treatment demonstrated an increased proportion of Nkx2-1/BrdU+ cells among the
356 $Braf^{V637E}$-expressing condition (4OHT) compared to the control (cAMP) (Figure 2C).

357 One of the hallmarks of thyroid cancer development is the downregulation of
358 thyroid differentiation markers (Mitsutake, 2005; Chakravarty, 2011). Indeed, the
359 activation of $Braf^{V637E}$ rapidly led to a progressive time-dependent decrease of *Tpo*, *TSHR*
360 and *Tg* mRNA expression (Figures 2D-F and S3B), detected as early as 6 hours after
361 4OHT addition (Figure 2D). Notably, more significant downregulation was observed
362 after 48 hours and maintained for at least 7 days (Figures 2E-F, respectively). As
363 described among PTCs, in our model, the expression of thyroid transcription factors *Pax8*
364 and *Nkx2-1* was also globally maintained. Conversely, *Lgals3 (Galectin 3)* expression,
365 which has been suggested as a marker for thyroid malignancies and, more specifically,
366 for PTC[67], was significantly increased in both time points (Figures 2E-F). Also, an
367 increase in Fibronectin 1 (*Fn1*) expression, associated with aggressive thyroid cancer[68,69],
368 was observed after 7 days of $Braf^{V637E}$ induction, suggesting a more advanced
369 dedifferentiated cell state in our organoid model (Figure 2F). Similar results were
370 obtained when cells were differentiated using hrTSH instead of cAMP, and $Braf^{V637E}$ was
371 induced in such conditioned media, indicating that the phenotype is not dependent of TSH
372 signaling (data not shown).

373 Histological analysis performed after 48 hours of continuous activation of
374 $Braf^{V637E}$ by 4OHT demonstrated disruption of the follicular organization in non-enriched
375 thyroid organoids compared to the control condition (cAMP) (Figure 3A). Nkx2-1 and

376 Tg staining revealed that Braf^{V637E} oncogene strongly disturbs thyroid follicles forming
377 elongated and unorganized structures. In addition, heterogeneous expression of Tg was
378 observed among the Nkx2-1 cells. Further analysis, performed in follicle enriched
379 population, confirmed the effect of *Braf* oncogene in promoting cell dedifferentiation and
380 loss of follicle organization. Tg levels were overall reduced and heterogeneous among
381 the unorganized Nkx2-1+ cells (Figure 3B). Interestingly, the cell disorganization caused
382 by Braf oncogene might pass by an initial expansion of the follicular size with infiltration
383 of Nkx2-1 cells inside of the lumen compartment, which also presents a heterogeneous
384 distribution of Tg (Figure S3C), since this feature was observed among some "follicular-
385 like" remaining structures after 48 h of 4OHT treatment. Reassuringly, staining for E-
386 Cadherin (epithelial) and Zo-1 (intra-luminal) adhesion markers showed that Braf^{V637E}-
387 expressing cells (Nkx2-1) are not able to preserve polarization and, consequently lumen
388 space is not well defined in most of the structures (Figures 3C-D, respectively). Therefore,
389 the functionality of those cells was impaired and, Tg-I accumulation was significantly
390 reduced compared to the control condition (Figure 3E). Of note, despite the strong effect
391 of Braf^{V637E} oncogene on thyroid follicles disruption, we observed that few follicles still
392 preserved a certain degree of organization (Figure S3D) after 48 h of 4OHT treatment.
393 As expected, after 7 days of Braf^{V637E} continuous stimulation, a higher level of cell
394 dedifferentiation and lack of organization could be detected, with a lower proportion of
395 the Nkx2-1 cells expressing Tg compared to control (Figure 3F) and to the previous time
396 point (48 h; Figure 3A). The above-described experiments were also performed using the
397 control TRE-Nkx2-1-Pax8_bTg-eGFP cell line. Adding 4OHT to mature follicles (from
398 day 27 to day 36) did not impair the levels of the thyroid differentiation markers and the
399 follicles organization (Figures S3E-F). On the other hand, slight induction of *Nkx2.1,*

400 *Pax8, Tg, TshR, Tpo and Nis* levels was observed under cAMP co-treatment with 4OHT
401 (Figure S3E).
402
403 *Effect of transient Braf^{V637E}-induction on cell differentiation*
404 Since our system for Braf^{V637E} activation is dependent on continuous treatment with
405 4OHT, we transiently treated the cells with 4OHT for 2 days, followed by 5 days of
406 culture in a 4OHT-free medium (cAMP) in order to explore if the oncogenic effect is
407 maintained when the protein is not active. Surprisingly, we did not observe the recovery
408 of *Nkx2-1, TSHR, Tg* or *Tpo* gene expression levels (Figures 4A-E) after 4OHT removal.
409 However, *Pax8* and *Slc5a5/Nis* expression was partially recovered (Figure 4F),
410 confirming the specific inhibitory effect of *Braf* oncogene on *Slc5a5/Nis* expression.
411 These findings indicate that *Nis* regulation mechanisms are maintained in our system and
412 suggest it as a tool for Nis-reactivation studies.
413
414 *Screening for Nis re-expression using signaling pathways inhibitors*
415 Studies in mouse models and humans have demonstrated that tumors carrying *Braf*
416 mutations show reduced expression of *Nis* and, consequently a higher rate of radioiodine
417 (RAI) refractoriness[28,31,65]. Here, taking advantage of our PTC organoid model, we aim
418 to explore new strategies to reactivate *Nis* expression in Braf^{V637E}-expressing cells by
419 screening distinct categories of inhibitors previously described to be involved in *Nis*
420 regulation [59,60]. PD0325901 (MEK inhibitor), LY204002 (PI3K inhibitor), VPA (HDAC
421 inhibitor), NAC (N-acetyl cysteine, antioxidant compound), 5-AZA-2' deoxycytidine and
422 RG108 (DMNT inhibitors) were tested isolated and/or in combination for 3 days (in
423 addition to cAMP+4OHT) using Braf^{V637E}-expressing organoids (after 4 days of
424 cAMP+4OHT treatment; Figure 5A). Initially, we observed that VPA alone was the only

425 treatment able to completely restore *Nis* expression levels (Figure 5B-C and S4A).
426 However, when combined, PD0325901 and LY204002 inhibitors; PD0325901,
427 LY204002 and VPA; and PD0325901 and Nac resulted in a great increase of *Nis* mRNA
428 (Figure 5B-C and S4A). IF staining shows Nis protein re-expression among Braf^{V637E}-
429 induced cells treated with VPA alone, but localization was not restricted to the membrane.
430 In contrast, when cells were treated with MEK of PI3K inhibitors, associated or not with
431 VPA, we observed Nis protein at the apical membrane and surprisingly, restored the
432 follicular structure (Figure 5C).
433
434 *MAPK and PI3K signaling inhibition cause Braf-induced cells redifferentiation and*
435 *function recovery*
436 Since we observed that HDAC, MEK and PI3K inhibition seems to favor follicle
437 reorganization, we evaluated if such treatments also induce cell redifferentiation and
438 function recovery. Initially, we analyzed the gene expression levels of thyroid
439 differentiation markers strongly affected by Braf-induction. The effects of isolated and
440 combined drugs on *Tg, TSHR, Tpo, Nkx2-1* and *Duox* genes appear variable and pathway-
441 dependent (Figure S4B-F). As with *Slc5a5/Nis*, MEK and PI3K inhibition in combination
442 with or without VPA resulted in complete recovery of *Tg*, *TSHR* and *Tpo* mRNA levels
443 (Figures 6A-C), indicating cell redifferentiation. While *TSHR* levels can be restored by
444 treatment with isolated inhibitors (Figure 6B), *Tpo* expression appears to be dependent
445 on PI3K signaling (Figure 6C). On the other hand, *Tg* mRNA expression is recovered just
446 when the inhibitors are used in combination (Figure 6A). Indeed, immunostaining showed
447 that isolated inhibitors could not restore Tg levels. Nevertheless, a higher proportion of
448 Tg-expressing cells was observed with the MEK inhibitor PD0325901 (Figure S4G).

449 Conversely, combined MEK and PI3K inhibitors restored Tg protein levels and generated
450 a similar proportion of expressing follicles as under the cAMP condition (Figures 6D-E).
451 Considering that inhibition of MEK and PI3K pathways (+/-VPA) promote recovery of
452 thyroid redifferentiation and follicular organization, we tested the functionality of
453 reorganized follicles. Remarkably, we observed an accumulation of Tg-I in the lumen of
454 follicles treated with the combinations of inhibitors (Figure 6F). The organification assay
455 confirmed that the co-treatment restored iodide uptake and ^{125}I binding to proteins
456 resulting in organification levels comparable to the control (Figure 6G-I).
457

458 *Transcriptomic characterization of the PTC model and drug screening tests*

459 Transcriptomic analysis of cAMP, cAMP+4OHT and cAMP+4OHT+PD+LY (Figure
460 5A) confirmed downregulation of thyroid genes under Braf-oncogene stimulation (4OHT
461 condition) whereas, global recovery of expression was observed under inhibitors
462 treatment (Figure 7A). Accordingly, thyroid differentiation scores (TDS and enhanced
463 (e)TDS) were decreased under Braf^{V637E} induction while they recovered in the presence
464 of inhibitors (Figure 7B). Conversely, the ERK activation score was higher in the
465 Braf^{V637E} samples and decreased sharply under inhibitor conditions (Figure 7C). Since
466 bulk RNAseq was performed using the follicle-enriched population, the presence of non-
467 thyroid cells is reduced compared with the whole original organoids but still present. It
468 may explain the modest increase in ERK score among Braf-activated cells while the
469 apparent decrease under the condition with inhibitors reflects the effect of the treatment
470 on each cell type.
471 Differential expression analysis identified 321 Differential Expressed Genes (DEGs; 156
472 upregulated and 165 downregulated genes) in the 4OHT condition compared to cAMP;
473 and 853 DEGs in inhibitors compared to 4OHT (287 upregulated and 566 downregulated

474 genes). Gene enrichment classification analysis of DEGs results is presented in Figures
475 7D-G. Briefly, among the upregulated genes in Braf-induced compared to control, we
476 observed gene signature for the hyperactivation of PI3K-AKT-mTOR, TNF and
477 cytokines signaling and promotion of Epithelial-Mesenchymal transition (EMT) (Figure
478 7D). While genes associated to thyroid hormone production, TGF-beta, Wnt/Beta-
479 Catenin pathway and regulation of angiogenesis were down-regulated (Figure 7E).
480 Conversely, the inhibitor's treatment, compared to 4OHT condition, evidenced
481 upregulation of genes associated to thyroid hormone production, cell-cell contact, extra-
482 cellular matrix organization and angiogenesis processes (Figure 7F), while PI3K, MAPK,
483 TNF, cytokines signaling, ECM-receptor interactions and EMT-related genes were
484 downregulated (Figure 7G).
485
486 **Discussion**
487 Here, we described a Braf-oncogene derived thyroid cancer organoid model
488 recapitulating patient tumor features. *In vitro* thyroid cancer models that recapitulate
489 tumor development and behavior can facilitate the identification of early tumor drivers
490 and enable the screening of several new drugs for the treatment of thyroid cancer without
491 the need to use too many animal models. Combining our previous thyroid organoid model
492 derived from mESCs with an inducible system, the $Braf^{V637E}$ oncogene could be induced
493 explicitly in mature Tg-expressing cells to obtain a 3D *in vitro* cancer model.
494 Overexpression of $Braf^{V637E}$ rapidly led to MAPK activation with increased pERK, cell
495 dedifferentiation and disruption of follicular organization. Similar effects have been
496 described in genetically modified mouse models[28,70,71]. Furthermore, the gene expression
497 signature of our cancer organoids confirmed the findings found in the PTC samples,

498 which also showed enrichment of genes associated to p53, focal adhesion, ECM-receptor
499 interactions, EMT and inflammatory pathways[72–74].

500 Activating mutations in the *BRAF* gene are found in approximately 7% of all solid
501 human tumors, particularly common in PTCs, ATCs and melanomas. In addition, they
502 have been reported less frequently in colorectal cancers (CRCs), lung cancers, pediatric
503 low-grade gliomas (PLGGs), glioblastomas, breast cancers and serous ovarian cancers[75–
504 81]. In PTCs and melanomas, $BRAF^{V600E}$ mutation seems to be associated with a higher
505 degree of dedifferentiation and more aggressive histological patterns. However, its
506 prognostic role is still debated as it was not found independently of histological
507 features[33,34]. Nevertheless, studies suggest that $BRAF^{V600E}$ might predict response to
508 tyrosine kinase inhibitors (TKIs) in melanoma and lung cancer[82,83].

509 Surgery remains the first choice for thyroid cancer therapy. Recommended post-
510 operative treatment includes TSH suppression and RAI ablation, particularly as adjuvant
511 treatment for patients at high risk for tumor recurrence and to treat patients with
512 persistent/recurrent or metastatic disease[84]. The benefit of RAI has been demonstrated in
513 patients by reducing the risk of recurrence and disease-related mortality[85]. However,
514 approximately two-thirds of metastatic DTC become radioiodine refractory (RR-DTC),
515 defined by the absence of iodine uptake or tumor progression despite uptake[86,87]. There
516 is no curative treatment for radioiodine refractory DTCs. The recommended first-line
517 systemic treatment when local therapies are not possible is targeted therapies using
518 mainly multitarget TKIs, such as Lenvatinib showed a progression-free survival of 18
519 months [65,88–90]. However, it leads to frequent resistance and adverse effects.

520 NIS, a basal membrane iodide transporter, plays a critical role in radioiodine
521 accumulation in DTC cells and its level is closely related to response to RAI (I^{131}) therapy.
522 Studies in mouse models and humans have shown that the presence of *BRAF* mutations

523 results in lower *Nis* levels and, consequently a higher rate of RAI-refractory tumours[28,31].
524 Here, we confirmed that this regulation is preserved in our cancer organoids, as disruption
525 of *Braf* activation led to in recovery of *Nis* levels. As TKIs, retinoic acids (RA), histone
526 deacetylase inhibitors (HDAC), peroxisome proliferator-activated receptor-gamma
527 (PPARG) have been tested to promote redifferentiation and *NIS* re-expression of RR-
528 DTCs, to suggest RAI treatment after a short, targeted treatment[88,91–93]. This strategy
529 could lead to tumor response while limiting adverse effects and, several clinical trials are
530 ongoing. However, the re-expression of NIS is insufficient to explain the response to
531 redifferentiation therapeutics and RAI treatment. Membrane trafficking and the cellular
532 machinery that concentrate and retain iodine must be preserved[94] in a follicular
533 organization. Our model is proving to be a potential tool for redifferentiation studies
534 because of its ability to test large sets and combinations of treatments and to assess
535 follicular reorganization and iodide organification capacity using a functional assay that
536 is likely to be more strongly associated with response to RAI treatment than *NIS* mRNA
537 levels. $Braf^{V637E}$-expressing cells treated with VPA, MAPK and PI3K inhibitors showed
538 re-expression of *Nis* and corresponding uptake of radioactive iodide. Interestingly, the
539 combination of inhibitors also promoted the restoration of thyroid markers, follicular
540 organization, and iodide organification ability. Interestingly, an ongoing clinical trial tests
541 the effect of BKM120, a PI3K inhibitor, in patients with progressive, metastatic,
542 refractory, follicular or poorly differentiated thyroid cancers (NCT01830504). However,
543 the association with MAPK inhibitors is still not evaluated in patients with thyroid cancer.
544 In *BRAF*-mutated tumors, studies have shown that the combination of TKIs
545 therapies appears more effective and circumvents primary and acquired resistance to TKI
546 therapy. Often, resistance is due to reactivation of the MAPK/ERK pathway or activation
547 of other signaling pathways such as PTEN, NF-1 or RAS. It may also result from the

548 hyperactivation of tyrosine kinase receptors, such as PDFRβ, IGF-1R and HGF, which
549 lead to activation of the AKT/PI3K pathway[95]. Studies in patients with advanced
550 melanoma carrying a $BRAF^{V600E}$ mutation have shown that combining BRAF and MEK
551 inhibitors resulted in a higher rate of complete/partial responses and median progression-
552 free survival compared with monotherapy groups[96–98]. Such significant results lead to the
553 use of drug combinations as standard treatment for the patients[99,100].

554 In summary, we have developed a Braf oncogene-expressing thyroid cancer in
555 vitro organoid model from mESCs that recapitulates transcriptomic and histological
556 features of PTCs at early and advanced stages. Moreover, we demonstrated that the
557 combination of MEK and PI3K inhibitors promotes *Nis* re-expression and cell re-
558 differentiation leading to the restoration of follicular structures and thyroid functionality.
559 Considering the robustness of this *in vitro* model, which allows controlled induction of
560 the major thyroid oncogene in a three-dimensional system, its efficiency and simplicity,
561 our model can be used to study mechanisms associated with thyroid cancer development
562 and progression, thyroid redifferentiation and drug screening.

563

564 **Acknowledgements and Funding**

565 The authors acknowledge the ULB flow cytometry platform (C. Dubois), the ULB
566 genomic core facility (F. Libert and A. Lefort), LiMIF platform for confocal microscopy
567 (J.-M. Vanderwinden). We acknowledge the funding agencies that supported this study.
568 The Belgian National Fund for Scientific Research (FNRS) (PDR T.0140.14; PDR
569 T.0230.18, CDR J.0068.22, Televie 7.4633.17/7.4526.19) and the Fonds
570 d'Encouragement à la Recherche de l'Université Libre de Bruxelles (FER-ULB). The
571 Belgian Fondation contre le cancer (F/2020/1402; V.D.). FNRS (Chargé de Recherche,
572 No.825745; M.R.). The cooperation program CAPES-WBI (S.C. and A.L.M). The

Brazilian National Council for Scientific and Technological Development (CNPq; M.R. and A.L.M), the Coordination for the Improvement of Higher Education Personnel (CAPES; M.R. and A.L.M), the Brazilian Society of Endocrinology and Metabolism (SBEM; M.R. and A.L.M) and the Fundação de Amparo à Pesquisa do Estado do Rio Grande do Sul (FAPERGS; A.L.M). S.C is Research Director at FNRS. M.R is researcher at ULB.

Author contributions

H.L., S.C. and M.R. developed the project, designed the experiments and analyzed the data. L.H., T.P., S.G. and J.H. generated the plasmids and the G4 Rosaluc mESC line. M.R. and A.S. generated the G4 RosaLuc TRE-Nkx2-1-Pax8_bTg-NES-Braf^{V637E}-ERT^{2} and TRE-Nkx2-1-Pax8_bTg-eGFP cell lines. H.L., M.R., B.F.F., A.S., O.M., L.C., M.K.P. B.A., L.C., performed the *in vitro* experiments and protocol set up. M.R. and P.G. obtained confocal images. H.L., M.R. and A.T. performed bulk RNA-Sequencing and analyzed the results. H.L. and A.T. performed the bioinformatics analysis. H.L. and M.R. wrote the first draft and, A.L.M. and S.C. edited the manuscript. S.C., M.R. and A.L.M. acquired funding for the project. All authors contributed to the article and approved the submitted version.

Competing interests

All authors declare no competing interests.

Correspondence and requests for materials should be addressed to Mírian Romitti.

References

598 1. Schutgens, F. & Clevers, H. Human Organoids: Tools for Understanding Biology
599 and Treating Diseases. *Annual Review of Pathology: Mechanisms of Disease* **15**,
600 211–234 (2020).
601 2. Clevers, H. Modeling Development and Disease with Organoids. *Cell* **165**, 1586–
602 1597 (2016).
603 3. Kim, J., Koo, B. K. & Knoblich, J. A. Human organoids: model systems for
604 human biology and medicine. *Nature Reviews Molecular Cell Biology* vol. 21
605 571–584 Preprint at https://doi.org/10.1038/s41580-020-0259-3 (2020).
606 4. Boj, S. F. *et al.* Organoid Models of Human and Mouse Ductal Pancreatic
607 Cancer. *Cell* **160**, 324–338 (2015).
608 5. Gao, D. *et al.* Organoid Cultures Derived from Patients with Advanced Prostate
609 Cancer. *Cell* **159**, 176–187 (2014).
610 6. Sato, T. *et al.* Long-term Expansion of Epithelial Organoids From Human Colon,
611 Adenoma, Adenocarcinoma, and Barrett's Epithelium. *Gastroenterology* **141**,
612 1762–1772 (2011).
613 7. van de Wetering, M. *et al.* Prospective Derivation of a Living Organoid Biobank
614 of Colorectal Cancer Patients. *Cell* **161**, 933–945 (2015).
615 8. Drost, J. & Clevers, H. Organoids in cancer research. *Nat Rev Cancer* **18**, 407–
616 418 (2018).
617 9. Gleave, A. M., Ci, X., Lin, D. & Wang, Y. A synopsis of prostate organoid
618 methodologies, applications, and limitations. *Prostate* **80**, 518–526 (2020).
619 10. Maenhoudt, N. & Vankelecom, H. Protocol for establishing organoids from
620 human ovarian cancer biopsies. *STAR Protoc* **2**, 100429 (2021).
621 11. Gunti, S., Hoke, A. T. K., Vu, K. P. & London, N. R. Organoid and Spheroid
622 Tumor Models: Techniques and Applications. *Cancers (Basel)* **13**, 874 (2021).
623 12. Saito, Y. *et al.* Development of a functional thyroid model based on an organoid
624 culture system. *Biochem Biophys Res Commun* **497**, 783–789 (2018).
625 13. Chen, D. *et al.* Papillary thyroid cancer organoids harboring BRAFV600E
626 mutation reveal potentially beneficial effects of BRAF inhibitor-based
627 combination therapies. *J Transl Med* **21**, 9 (2023).
628 14. Vlachogiannis, G. *et al.* Patient-derived organoids model treatment response of
629 metastatic gastrointestinal cancers. *Science (1979)* **359**, 920–926 (2018).
630 15. Drost, J. *et al.* Sequential cancer mutations in cultured human intestinal stem
631 cells. *Nature* **521**, 43–47 (2015).
632 16. Matano, M. *et al.* Modeling colorectal cancer using CRISPR-Cas9–mediated
633 engineering of human intestinal organoids. *Nat Med* **21**, 256–262 (2015).
634 17. Miura, A. *et al.* Oncogenic potential of human pluripotent stem cell-derived lung
635 organoids with <scp>HER2</scp> overexpression. *Int J Cancer* **149**, 1593–1604
636 (2021).
637 18. Nadauld, L. D. *et al.* Metastatic tumor evolution and organoid modeling
638 implicate TGFBR2as a cancer driver in diffuse gastric cancer. *Genome Biol* **15**,
639 428 (2014).
640 19. Li, X. *et al.* Oncogenic transformation of diverse gastrointestinal tissues in
641 primary organoid culture. *Nat Med* **20**, 769–777 (2014).
642 20. Huang, L. *et al.* Ductal pancreatic cancer modeling and drug screening using
643 human pluripotent stem cell– and patient-derived tumor organoids. *Nat Med* **21**,
644 1364–1371 (2015).
645 21. Lo, Y.-H., Karlsson, K. & Kuo, C. J. Applications of organoids for cancer
646 biology and precision medicine. *Nat Cancer* **1**, 761–773 (2020).

647 22. Lim, H., Devesa, S. S., Sosa, J. A., Check, D. & Kitahara, C. M. Trends in
648 Thyroid Cancer Incidence and Mortality in the United States, 1974-2013. *JAMA*
649 **317**, 1338 (2017).
650 23. ROMITTI, M. *et al.* Signaling pathways in follicular cell-derived thyroid
651 carcinomas. *Int J Oncol* **42**, 19–28 (2013).
652 24. Kimura, E. T. *et al.* High prevalence of BRAF mutations in thyroid cancer:
653 genetic evidence for constitutive activation of the RET/PTC-RAS-BRAF
654 signaling pathway in papillary thyroid carcinoma. *Cancer Res* **63**, 1454–7
655 (2003).
656 25. Fagin, J. A. & Mitsiades, N. Molecular pathology of thyroid cancer: diagnostic
657 and clinical implications. *Best Pract Res Clin Endocrinol Metab* **22**, 955–969
658 (2008).
659 26. Scheffel, R. S. *et al.* The BRAFV600E mutation analysis and risk stratification in
660 papillary thyroid carcinoma. *Arch Endocrinol Metab* (2020) doi:10.20945/2359-
661 3997000000285.
662 27. Xing, M. The T1799A BRAF mutation is not a germline mutation in familial
663 nonmedullary thyroid cancer. *Clin Endocrinol (Oxf)* **63**, 263–266 (2005).
664 28. Chakravarty, D. *et al.* Small-molecule MAPK inhibitors restore radioiodine
665 incorporation in mouse thyroid cancers with conditional BRAF activation.
666 *Journal of Clinical Investigation* **121**, 4700–4711 (2011).
667 29. Zaman, Wu & Bivona. Targeting Oncogenic BRAF: Past, Present, and Future.
668 *Cancers (Basel)* **11**, 1197 (2019).
669 30. Agrawal, N. *et al.* Integrated Genomic Characterization of Papillary Thyroid
670 Carcinoma. *Cell* **159**, 676–690 (2014).
671 31. Romei, C. *et al.* Modifications in the Papillary Thyroid Cancer Gene Profile Over
672 the Last 15 Years. *J Clin Endocrinol Metab* **97**, E1758–E1765 (2012).
673 32. Sabra, M. M. *et al.* Clinical Outcomes and Molecular Profile of Differentiated
674 Thyroid Cancers With Radioiodine-Avid Distant Metastases. *J Clin Endocrinol*
675 *Metab* **98**, E829–E836 (2013).
676 33. Xing, M. BRAFV600E Mutation and Papillary Thyroid Cancer. *JAMA* **310**, 535
677 (2013).
678 34. Scheffel, R. S. *et al.* The BRAFV600E mutation analysis and risk stratification in
679 papillary thyroid carcinoma. *Arch Endocrinol Metab* (2021) doi:10.20945/2359-
680 3997000000285.
681 35. Liu, R. *et al.* Mortality Risk Stratification by Combining *BRAF* V600E and *TERT*
682 Promoter Mutations in Papillary Thyroid Cancer. *JAMA Oncol* **3**, 202 (2017).
683 36. Boucai, L. *et al.* Characterization of Subtypes of BRAF-Mutant Papillary
684 Thyroid Cancer Defined by Their Thyroid Differentiation Score. *J Clin*
685 *Endocrinol Metab* **107**, 1030–1039 (2022).
686 37. Antonica, F. *et al.* Generation of functional thyroid from embryonic stem cells.
687 *Nature* **491**, 66–71 (2012).
688 38. Romitti, M. *et al.* Transplantable human thyroid organoids generated from
689 embryonic stem cells to rescue hypothyroidism. *Nat Commun* **13**, 7057 (2022).
690 39. Longmire, T. A. *et al.* Efficient derivation of purified lung and thyroid
691 progenitors from embryonic stem cells. *Cell Stem Cell* **10**, 398–411 (2012).
692 40. Ma, R., Latif, R. & Davies, T. F. Human embryonic stem cells form functional
693 thyroid follicles. *Thyroid* **25**, 455–461 (2015).
694 41. Ma, R., Latif, R. & Davies, T. F. Thyroid follicle formation and thyroglobulin
695 expression in multipotent endodermal stem cells. *Thyroid* **23**, 385–391 (2013).

42. Ma, R., Morshed, S. A., Latif, R. & Davies, T. F. TAZ Induction Directs Differentiation of Thyroid Follicular Cells from Human Embryonic Stem Cells. *Thyroid* **27**, 292–299 (2017).
43. Ma, R., Shi, R., Morshed, S. A., Latif, R. & Davies, T. F. Derivation and 97% Purification of Human Thyroid Cells From Dermal Fibroblasts. *Front Endocrinol (Lausanne)* **11**, 446 (2020).
44. Kurmann, A. A. *et al.* Regeneration of Thyroid Function by Transplantation of Differentiated Pluripotent Stem Cells. *Cell Stem Cell* **17**, 527–542 (2015).
45. Serra, M. *et al.* Pluripotent stem cell differentiation reveals distinct developmental pathways regulating Lung-Versus Thyroid-Lineage specification. *Development (Cambridge)* **144**, 3879–3893 (2017).
46. Dame, K. *et al.* Thyroid Progenitors Are Robustly Derived from Embryonic Stem Cells through Transient, Developmental Stage-Specific Overexpression of Nkx2-1. *Stem Cell Reports* **8**, 216–225 (2017).
47. Ogundipe, V. M. L. *et al.* Generation and Differentiation of Adult Tissue-Derived Human Thyroid Organoids. *Stem Cell Reports* **16**, 913–925 (2021).
48. Liang, J. *et al.* Modeling Human Thyroid Development by Fetal Tissue-Derived Organoid Culture. *Advanced Science* **9**, (2022).
49. van der Vaart, J. *et al.* Adult mouse and human organoids derived from thyroid follicular cells and modeling of Graves' hyperthyroidism. *Proceedings of the National Academy of Sciences* **118**, (2021).
50. Chen, D. *et al.* Organoid Cultures Derived From Patients With Papillary Thyroid Cancer. *J Clin Endocrinol Metab* **106**, 1410–1426 (2021).
51. Sondorp, L. H. J. *et al.* Patient-Derived Papillary Thyroid Cancer Organoids for Radioactive Iodine Refractory Screening. *Cancers (Basel)* **12**, 3212 (2020).
52. Pecce, V. *et al.* Establishment and maintenance of thyroid organoids from human cancer cells. *STAR Protoc* **3**, 101393 (2022).
53. Chen, D. *et al.* Papillary thyroid cancer organoids harboring BRAFV600E mutation reveal potentially beneficial effects of BRAF inhibitor-based combination therapies. *J Transl Med* **21**, 9 (2023).
54. Yang, H. *et al.* Establishment of papillary thyroid cancer organoid lines from clinical specimens. *Front Endocrinol (Lausanne)* **14**, (2023).
55. Veschi, V. *et al.* Recapitulating thyroid cancer histotypes through engineering embryonic stem cells. *Nat Commun* **14**, 1351 (2023).
56. Haenebalcke, L. *et al.* Efficient ROSA26-Based Conditional and/or Inducible Transgenesis Using RMCE-Compatible F1 Hybrid Mouse Embryonic Stem Cells. *Stem Cell Rev Rep* **9**, 774–785 (2013).
57. Romitti, M. *et al.* Single-Cell Trajectory Inference Guided Enhancement of Thyroid Maturation In Vitro Using TGF-Beta Inhibition. *Front Endocrinol (Lausanne)* **12**, (2021).
58. Ortiz, O., Wurst, W. & Kühn, R. Reversible and tissue-specific activation of MAP kinase signaling by tamoxifen in braf ^{V637} ER ^{T2} mice. *genesis* **51**, 448–455 (2013).
59. Azouzi, N. *et al.* NADPH Oxidase NOX4 Is a Critical Mediator of BRAF ^{V600E} -Induced Downregulation of the Sodium/Iodide Symporter in Papillary Thyroid Carcinomas. *Antioxid Redox Signal* **26**, 864–877 (2017).
60. Kogai, T. & Brent, G. A. The sodium iodide symporter (NIS): Regulation and approaches to targeting for cancer therapeutics. *Pharmacol Ther* **135**, 355–370 (2012).

745 61. Bolger, A. M., Lohse, M. & Usadel, B. Trimmomatic: a flexible trimmer for
746 Illumina sequence data. *Bioinformatics* **30**, (2014).
747 62. Kim, D., Langmead, B. & Salzberg, S. L. HISAT: a fast spliced aligner with low
748 memory requirements. *Nat Methods* **12**, (2015).
749 63. Hao, Y. *et al.* Integrated analysis of multimodal single-cell data. *Cell* **184**, 3573-
750 3587.e29 (2021).
751 64. Love, M. I., Huber, W. & Anders, S. Moderated estimation of fold change and
752 dispersion for RNA-seq data with DESeq2. *Genome Biol* **15**, 550 (2014).
753 65. Dunn, L. A. *et al.* Vemurafenib Redifferentiation of *BRAF* Mutant, RAI-
754 Refractory Thyroid Cancers. *J Clin Endocrinol Metab* **104**, 1417–1428 (2019).
755 66. Antonica, F., Kasprzyk, D. F., Schiavo, A. A., Romitti, M. & Costagliola, S.
756 Generation of Functional Thyroid Tissue Using 3D-Based Culture of Embryonic
757 Stem Cells. in 85–95 (2017). doi:10.1007/978-1-4939-6949-4_7.
758 67. Tang, W.-W., Huang, C., Tang, C., Xu, J. & Wang, H. Galectin-3 may serve as a
759 potential marker for diagnosis and prognosis in papillary thyroid carcinoma: a
760 meta-analysis. *Onco Targets Ther* 455 (2016) doi:10.2147/OTT.S94514.
761 68. Xia, S. *et al.* Fibronectin 1 promotes migration and invasion of papillary thyroid
762 cancer and predicts papillary thyroid cancer lymph node metastasis. *Onco*
763 *Targets Ther* **Volume 10**, 1743–1755 (2017).
764 69. Sponziello, M. *et al.* Fibronectin-1 expression is increased in aggressive thyroid
765 cancer and favors the migration and invasion of cancer cells. *Mol Cell*
766 *Endocrinol* **431**, 123–132 (2016).
767 70. Knauf, J. A. *et al.* Targeted Expression of BRAFV600E in Thyroid Cells of
768 Transgenic Mice Results in Papillary Thyroid Cancers that Undergo
769 Dedifferentiation. *Cancer Res* **65**, 4238–4245 (2005).
770 71. Saqcena, M. *et al.* SWI/SNF Complex Mutations Promote Thyroid Tumor
771 Progression and Insensitivity to Redifferentiation Therapies. *Cancer Discov* **11**,
772 1158–1175 (2021).
773 72. Qiu, W., Yang, Z., Fan, Y. & Zheng, Q. ZNRF3 is downregulated in papillary
774 thyroid carcinoma and suppresses the proliferation and invasion of papillary
775 thyroid cancer cells. *Tumor Biology* **37**, 12665–12672 (2016).
776 73. Han, J. *et al.* Identification of Biomarkers Based on Differentially Expressed
777 Genes in Papillary Thyroid Carcinoma. *Sci Rep* **8**, 9912 (2018).
778 74. Yoo, S.-K. *et al.* Integrative analysis of genomic and transcriptomic
779 characteristics associated with progression of aggressive thyroid cancer. *Nat*
780 *Commun* **10**, 2764 (2019).
781 75. Davies, H. *et al.* Mutations of the BRAF gene in human cancer. *Nature* **417**,
782 949–954 (2002).
783 76. Dhomen, N. & Marais, R. New insight into BRAF mutations in cancer. *Curr*
784 *Opin Genet Dev* **17**, 31–39 (2007).
785 77. Nikiforov, Y. E. & Nikiforova, M. N. Molecular genetics and diagnosis of
786 thyroid cancer. *Nat Rev Endocrinol* **7**, 569–580 (2011).
787 78. Cheng, L., Lopez-Beltran, A., Massari, F., MacLennan, G. T. & Montironi, R.
788 Molecular testing for BRAF mutations to inform melanoma treatment decisions:
789 a move toward precision medicine. *Modern Pathology* **31**, 24–38 (2018).
790 79. Schirripa, M. *et al.* Class 1, 2, and 3 BRAF-Mutated Metastatic Colorectal
791 Cancer: A Detailed Clinical, Pathologic, and Molecular Characterization.
792 *Clinical Cancer Research* **25**, 3954–3961 (2019).
793 80. Pisapia, P., Pepe, F., Malapelle, U. & Troncone, G. Mutations in Lung Cancer.
794 *Acta Cytol* **63**, 247–250 (2019).

81. Pisapia, P. *et al.* BRAF: A Two-Faced Janus. *Cells* **9**, 2549 (2020).
82. Pavlick, A. C., Fecher, L., Ascierto, P. A. & Sullivan, R. J. Frontline Therapy for BRAF-Mutated Metastatic Melanoma: How Do You Choose, and Is There One Correct Answer? *American Society of Clinical Oncology Educational Book* 564–571 (2019) doi:10.1200/EDBK_243071.
83. Anguera, G. & Majem, M. BRAF inhibitors in metastatic non-small cell lung cancer. *J Thorac Dis* **10**, 589–592 (2018).
84. Haugen, B. R. *et al.* 2015 American Thyroid Association Management Guidelines for Adult Patients with Thyroid Nodules and Differentiated Thyroid Cancer: The American Thyroid Association Guidelines Task Force on Thyroid Nodules and Differentiated Thyroid Cancer. *Thyroid* **26**, 1–133 (2016).
85. Schmidbauer, B., Menhart, K., Hellwig, D. & Grosse, J. Differentiated Thyroid Cancer—Treatment: State of the Art. *Int J Mol Sci* **18**, 1292 (2017).
86. Kim, T. Y., Kim, W. G., Kim, W. B. & Shong, Y. K. Current Status and Future Perspectives in Differentiated Thyroid Cancer. *Endocrinology and Metabolism* **29**, 217 (2014).
87. Ahn, B.-C. Personalized Medicine Based on Theranostic Radioiodine Molecular Imaging for Differentiated Thyroid Cancer. *Biomed Res Int* **2016**, 1–9 (2016).
88. Paeng, J. C., Kang, K. W., Park, D. J., Oh, S. W. & Chung, J.-K. Alternative Medical Treatment for Radioiodine-Refractory Thyroid Cancers. *Nucl Med Mol Imaging* **45**, 241–247 (2011).
89. Brose, M. S. *et al.* Sorafenib in radioactive iodine-refractory, locally advanced or metastatic differentiated thyroid cancer: a randomised, double-blind, phase 3 trial. *The Lancet* **384**, 319–328 (2014).
90. Schlumberger, M. *et al.* Lenvatinib versus Placebo in Radioiodine-Refractory Thyroid Cancer. *New England Journal of Medicine* **372**, 621–630 (2015).
91. Ho, A. L. *et al.* Selumetinib-Enhanced Radioiodine Uptake in Advanced Thyroid Cancer. *New England Journal of Medicine* **368**, 623–632 (2013).
92. Rothenberg, S. M., Daniels, G. H. & Wirth, L. J. Redifferentiation of Iodine-Refractory BRAF V600E-Mutant Metastatic Papillary Thyroid Cancer with Dabrafenib—Response. *Clinical Cancer Research* **21**, 5640–5641 (2015).
93. Buffet, C. *et al.* Redifferentiation of radioiodine-refractory thyroid cancers. *Endocr Relat Cancer* **27**, R113–R132 (2020).
94. Riesco-Eizaguirre, G. & Santisteban, P. A perspective view of sodium iodide symporter research and its clinical implications. *Eur J Endocrinol* **155**, 495–512 (2006).
95. Czarnecka, A. M., Bartnik, E., Fiedorowicz, M. & Rutkowski, P. Targeted Therapy in Melanoma and Mechanisms of Resistance. *Int J Mol Sci* **21**, 4576 (2020).
96. Flaherty, K. T. *et al.* Combined BRAF and MEK Inhibition in Melanoma with BRAF V600 Mutations. *New England Journal of Medicine* **367**, 1694–1703 (2012).
97. Larkin, J. *et al.* Combined Vemurafenib and Cobimetinib in BRAF-Mutated Melanoma. *New England Journal of Medicine* **371**, 1867–1876 (2014).
98. Dummer, R. *et al.* Encorafenib plus binimetinib versus vemurafenib or encorafenib in patients with BRAF -mutant melanoma (COLUMBUS): a multicentre, open-label, randomised phase 3 trial. *Lancet Oncol* **19**, 603–615 (2018).
99. Smalley, K. S. M. Increased immunity and BRAF inhibition: Yet another argument for combination therapy? *Pharmacol Res* **113**, 719–720 (2016).

100. Roskoski, R. Targeting oncogenic Raf protein-serine/threonine kinases in human cancers. *Pharmacol Res* **135**, 239–258 (2018).

871 **Figures**

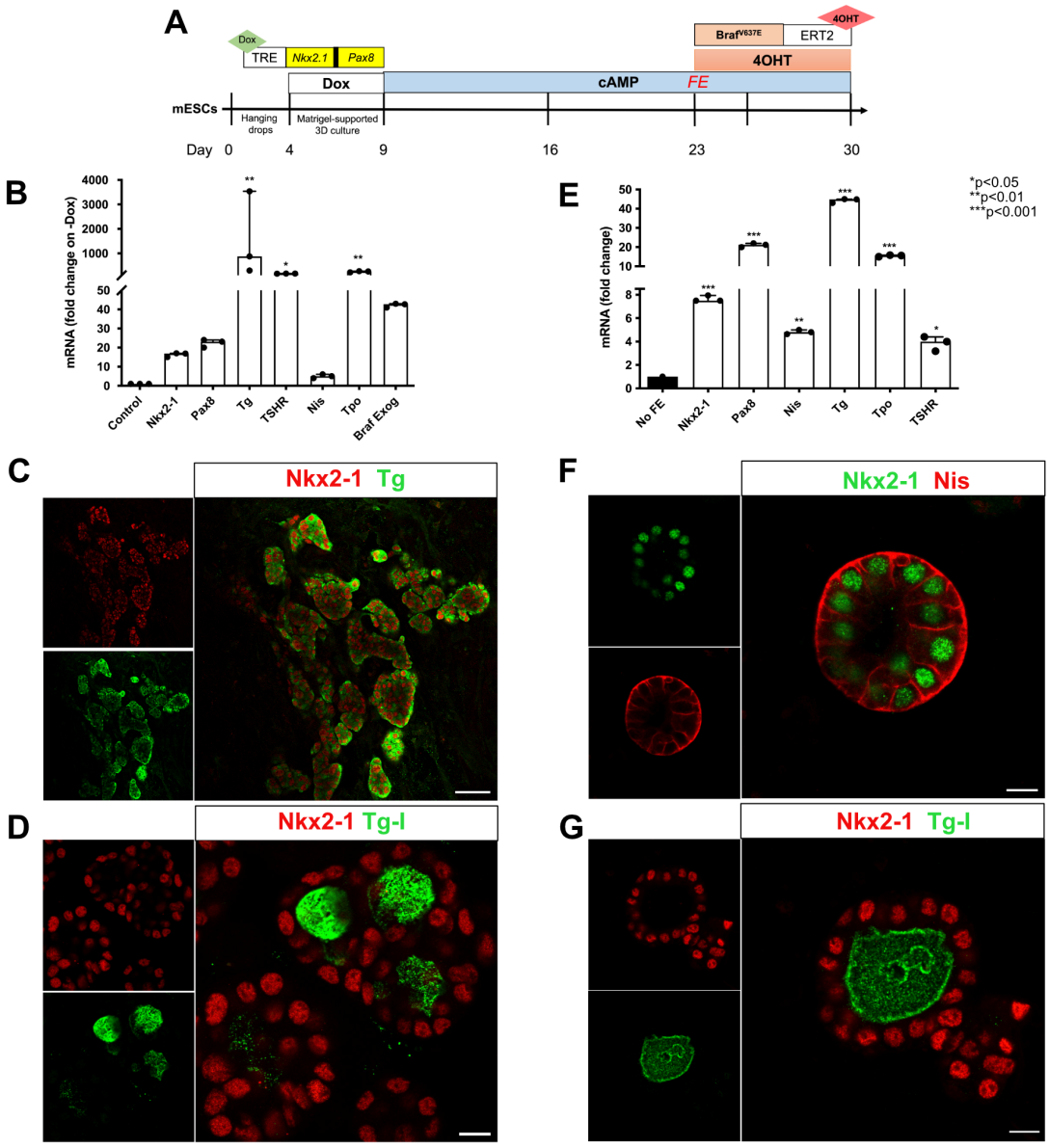

872

873 **Figure 1. mESC_Nkx2-1/Pax8_bTg_Braf^{V637E} cell line differentiation into thyroid**
874 **organoids.** Scheme of the thyroid differentiation protocol and Braf^{V637E} induction in
875 mature thyroid follicles (A). Differentiation of mESC_Nkx2-1/Pax8_bTg_Braf^{V637E} cell
876 line promotes expression of the main thyroid genes and Braf exogenous (B).
877 Immunofluorescence staining showing Nkx2-1 and Tg co-expressing cells organized in
878 follicular structures (C), which are accumulating the thyroid hormone precursor, Tg-I,
879 inside the lumen compartment (D). The follicular enrichment (FE) procedure
880 significantly increased the expression levels of thyroid genes (E) while keeping the

881 structural organization of the follicles (F) and its functionality evidenced by Tg-I

882 accumulation (G). Scale bars, 50 µm and 10 µm for high magnification follicles.

883

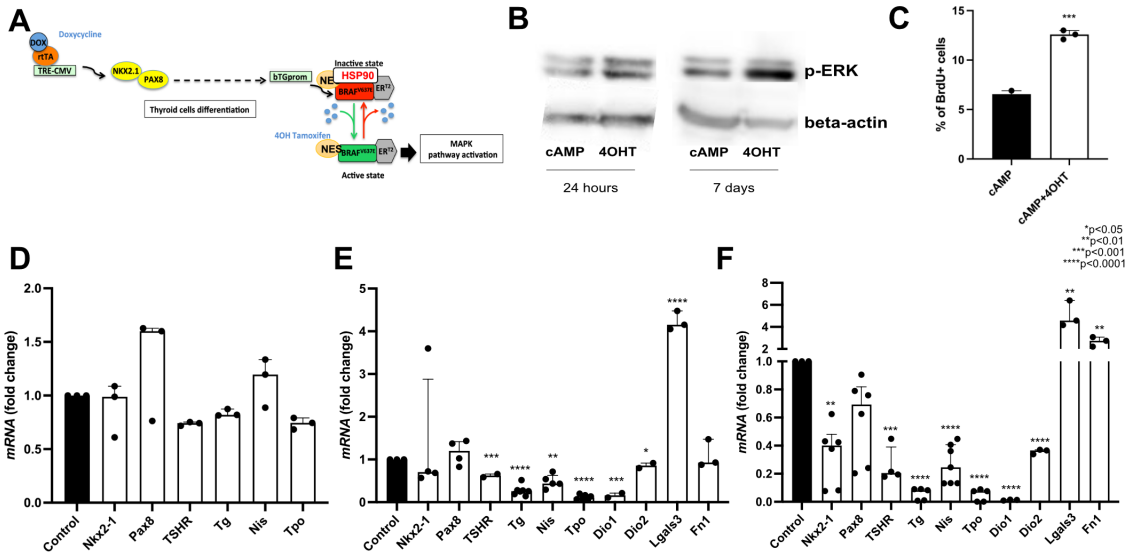

884

885 **Figure 2. Effect of the Braf^{V637E} oncogene induction on mature thyroid follicles.**

886 Schematic representation of thyroid differentiation, Braf^{V637E} oncogene expression and

887 its activation under specific treatment conditions (A). Western blot demonstrates an

888 increase of p-ERK protein at 24 hours and 7 days after the addition of 4OHT (Tamoxifen)

889 to the organoids culture (B). Percentage of BrDU+ cells between control (cAMP) and

890 Braf-induced (4OHT; 6 days) condition (C). mRNA expression analysis showing the

891 inhibitory effect of Braf^{V637E}-oncogene induction on thyroid genes after 6 hours (D), 48

892 hours (E) and 7 days (F).

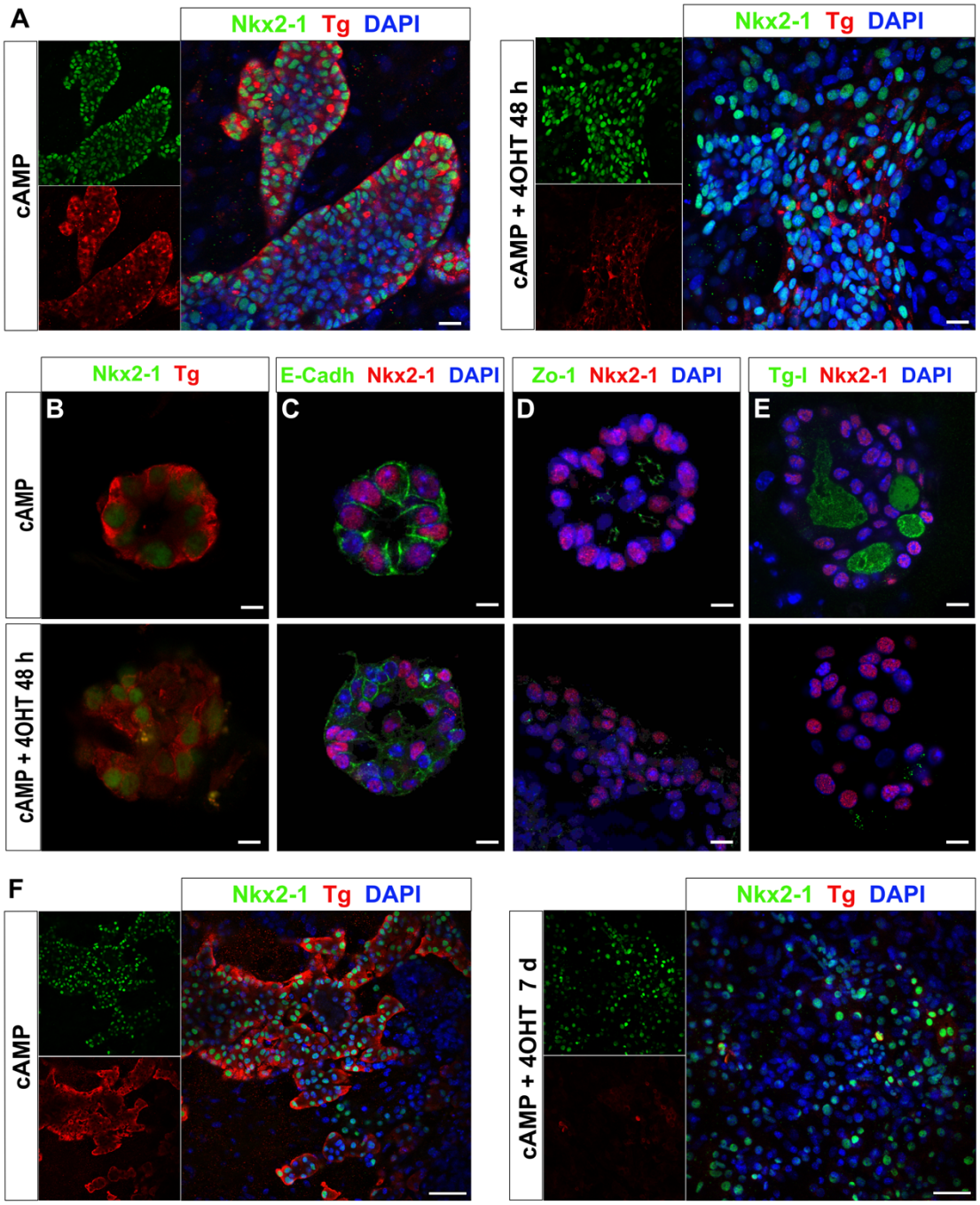

Figure 3. Morphological changes caused by Braf^{V637E} activation on thyroid follicles. Control thyroid cells show follicular organization with Nkx2-1 nuclear expression and Tg accumulation in the luminal compartment. In contrast, after 48 h of Braf oncogene induction by 4OHT, most of the cells are not organized into follicular structures and a great proportion of cells is expressing very low levels of Tg (A). Higher magnification images showing the follicular organization of the thyroid cells in the control condition

900 (48 h), with proper expression of Nk2x-1 and/or Tg (B), E-cadherin (C), Zo-1 (D) and
901 Tg-I (E) accumulation in the lumen. While in the 4OHT condition the follicular
902 organization is disrupted as well as its function. Nkx2-1 and Tg staining in control and
903 Braf-induced cells for 7 days shows clear changes in thyroid morphology evidenced by
904 the heterogeneity of Nkx2-1 cells which mostly do not express Tg or at low levels, while
905 some groups cells continue to co-express Tg (F). Scale bars, 20 µm (A), 10 µm (B-E) and
906 50 µm (F).
907

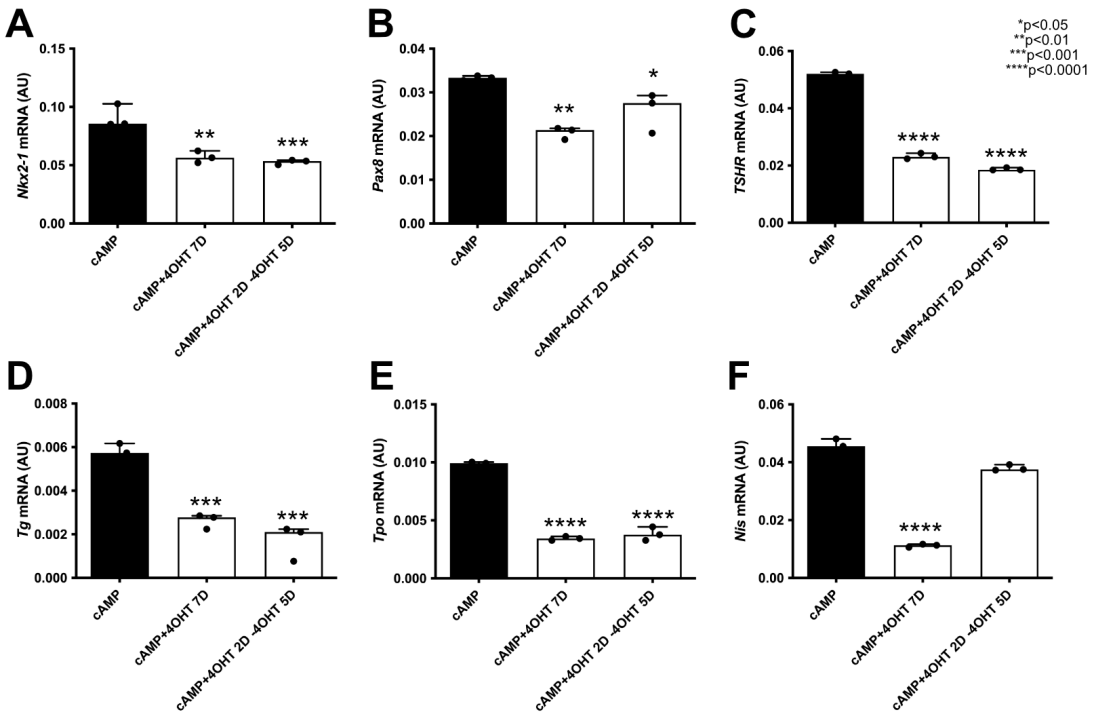

908

909 **Figure 4. 4OHT interruption does not restore the thyroid gene expression levels.** The
910 induction of Braf^{V637E} for 2 days followed by removal of 4OHT for 5 days shows that it
911 is not enough to recover the levels of *Nkx2-1* (A), *Pax8* (B), *TSHR* (C), *Tg* (D), *Tpo* (E)
912 genes to the control levels. However, it led to an increase of *Nis* expression (F) close to
913 control values.

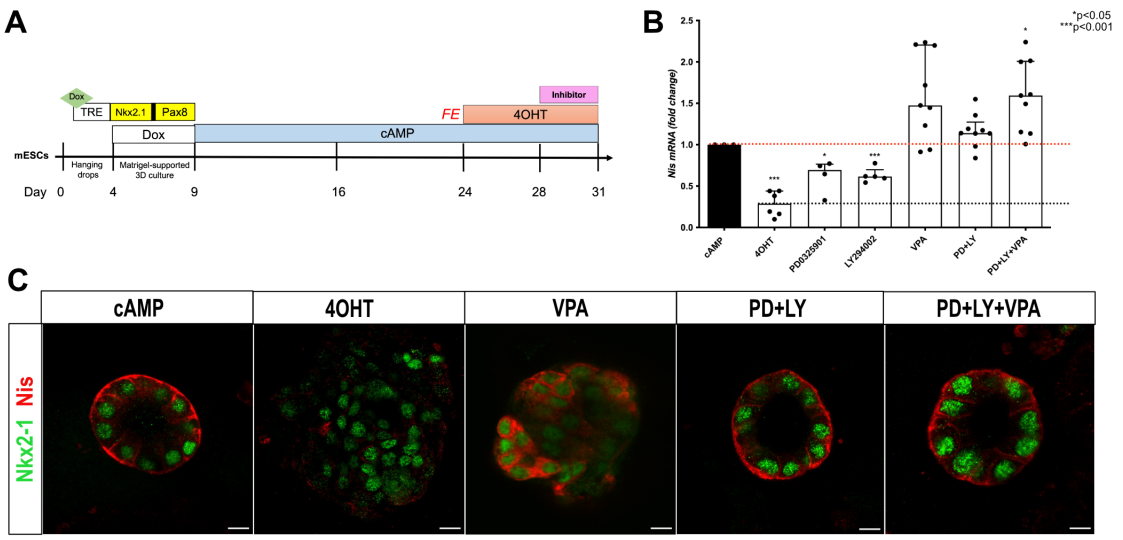

914

915 **Figure 5. Drug screening reveals that VPA and MAPK/PI3K inhibition can restore**

916 **Nis expression in Braf-induced cells.** Schematic representation of the protocol used for

917 drug screening experiments (A). qPCR data show that inhibition of MAPK (PD0325901)

918 and PI3K (LY294002) pathways isolated increase but do not restore *Nis* expression to

919 control levels. However, when combined, the levels are like the controls. On the other

920 hand, the HDAC inhibitor (VPA) can recover Nis expression (B) by itself. Nkx2-1 and

921 Nis immunostaining shows the downregulation of the transporter in 4OHT condition,

922 which is restored by VPA treatment. However, the expression pattern differs from the

923 control conditions. Co-inhibition of MAPK and PI3K pathways associated or not to VPA

924 treatment restores of Nis protein expression while follicular structures are observed (C).

925 Scale bars, 10 µm.

926

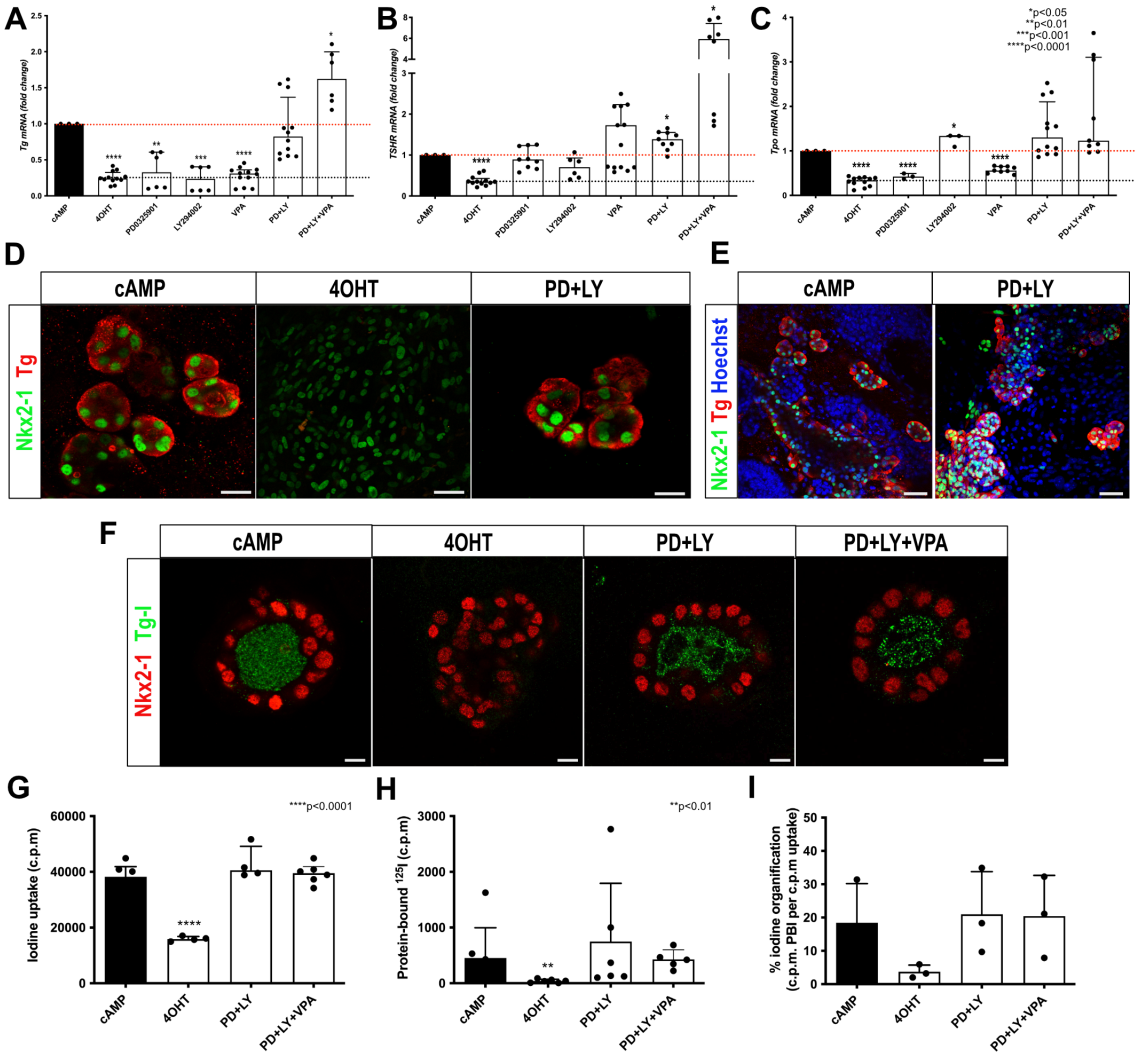

927

928 **Figure 6. MAPK and PI3K inhibition cause thyroid redifferentiation and function**
929 **recovery of Braf-expressing cells.** mRNA expression analysis shows that PD0325901
930 and LY294002 co-treatment recover the *Tg* (A), *TSHR* (B), and *Tpo* (C) gene expression
931 to control levels. Immunostaining for Nkx2-1 and Tg shows that protein levels are similar
932 to control and that follicular organization is restored under such treatment conditions (D,
933 E). Tg-I accumulation in the lumen of the restored follicles is observed under PD+LY
934 and PD+LY+VPA conditions (F). Organification assay shows a recovery of Iodine uptake
935 (G), Protein-bound to 125I (H), and % of iodine Organification (I) in the inhibitor's
936 conditions. Scale bars, 50 µm (E), 20 µm (D) and 10 µm for high magnification follicles
937 (F).

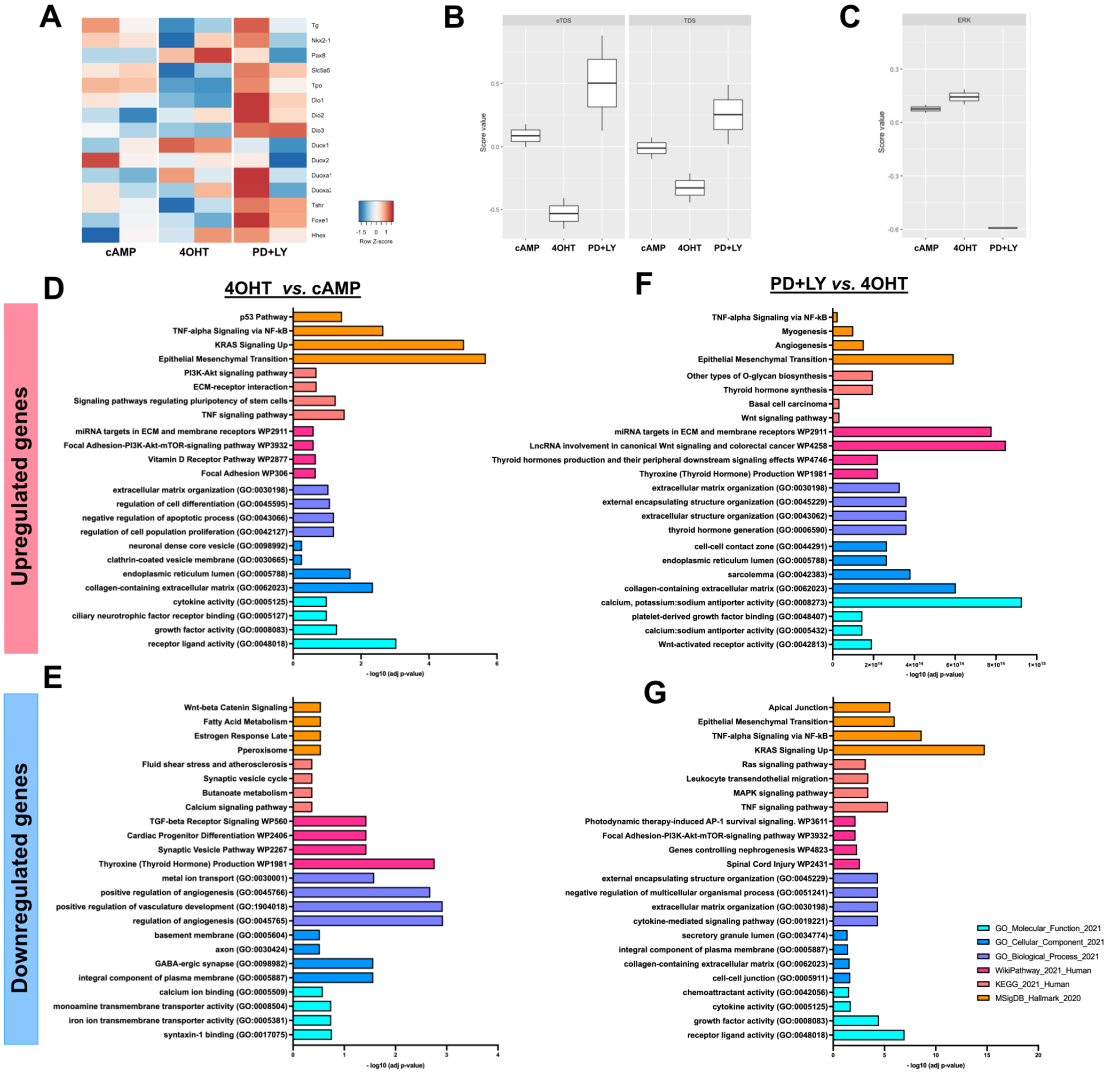

Figure 7. Transcriptomics analysis confirms thyroid redifferentiation of Braf^{V637E}-expressing cells treated with MAPK and PI3K inhibitors and suggests by which mechanisms. Heatmap of normalized bulk RNA-Seq expression of normal thyroid cells (cAMP), Braf^{V637E} expressing cells (4OHT), and Braf^{V637E} expressing cells treated with PD0325901+LY204002 inhibitors. Rows represent markers and columns represent specific conditions. Color values in the heatmap represent mean expression levels (A). Thyroid differentiation (eTDS and TDS) (B) and ERK (C) scores were calculated among the different conditions. Classification of upregulated and downregulated genes comparing 4OHT *vs.* cAMP (D, E) and PD+LY *vs.* 4OHT (F, G). Colors represent the classification method and scale the -log10 (adj p-value).

949 **Supplementary data**

950

951 Supplementary figures

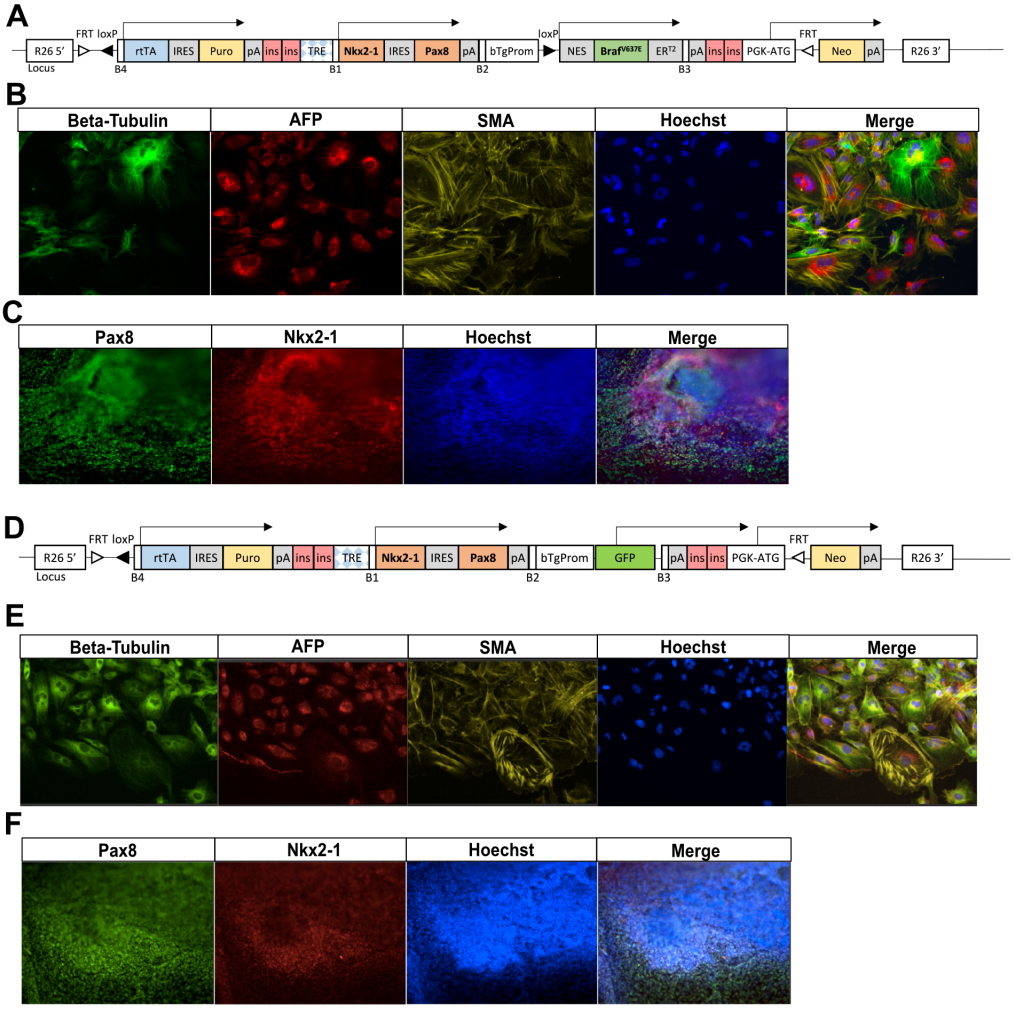

952

953 **Figure S1. mESC-cell lines generation and characterization.** Schematic representation
954 of the mESC_Nkx2-1/Pax8_bTg_Braf^{V637E} cell line (A). mESC_Nkx2-
955 1/Pax8_bTg_Braf^{V637E} line response to doxycycline treatment shows expression of Pax8
956 and Nkx2-1 proteins (B). Spontaneous differentiation mESC_Nkx2-
957 1/Pax8_bTg_Braf^{V637E} cell line leads to the generation of ectodermal (Beta-actin),
958 endodermal (AFP) and mesodermal (SMA) cells (C). Schematic representation of the
959 mESC_Nkx2-1/Pax8_bTg_eGFP control cell line (D). Dox treatment leads to an increase
960 of Pax8 and Nkx2-1 expression in control cells (E). Spontaneous differentiation of the

961 control cells leads to generation of ectodermal (Beta-actin), endodermal (AFP) and
962 mesodermal (SMA) cells (F). Scale bars, 50 µm (B, E) and 10 µm (C, F).
963

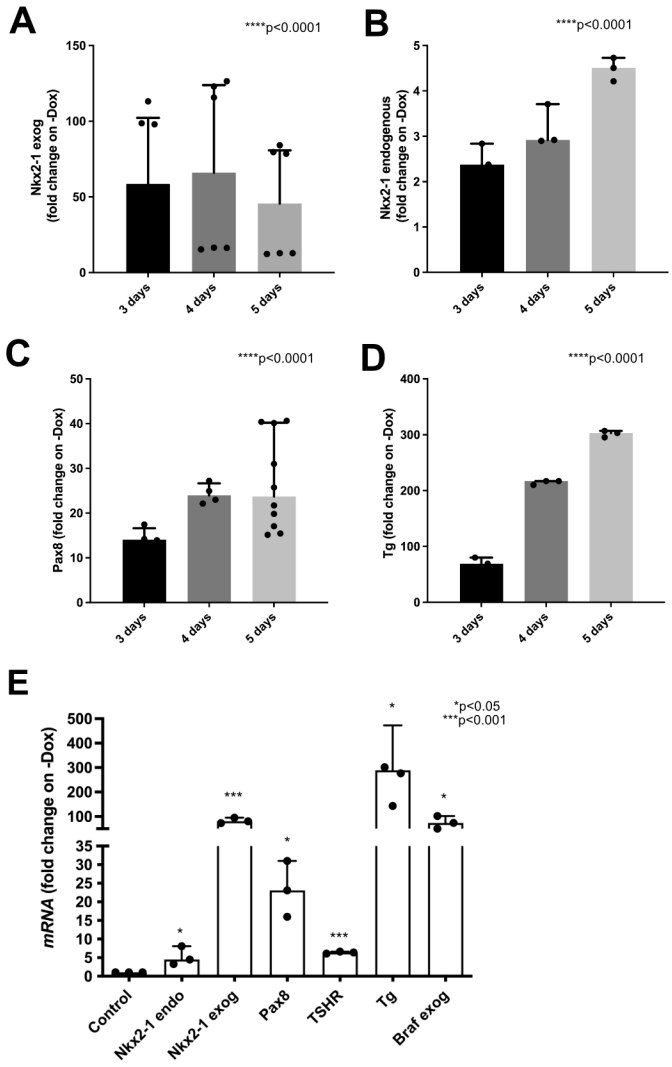

964

965 **Figure S2. Doxycycline treatment for 5 days leads to more efficient thyroid gene**
966 **expression induction.** Time course of Dox-dependent induction of exogenous and
967 endogenous *Nkx2-1* (A, B) *Pax8* (C) and *Tg* (D) expression. mRNA levels of thyroid
968 genes at day 9, after 5 days of Dox treatment (E).

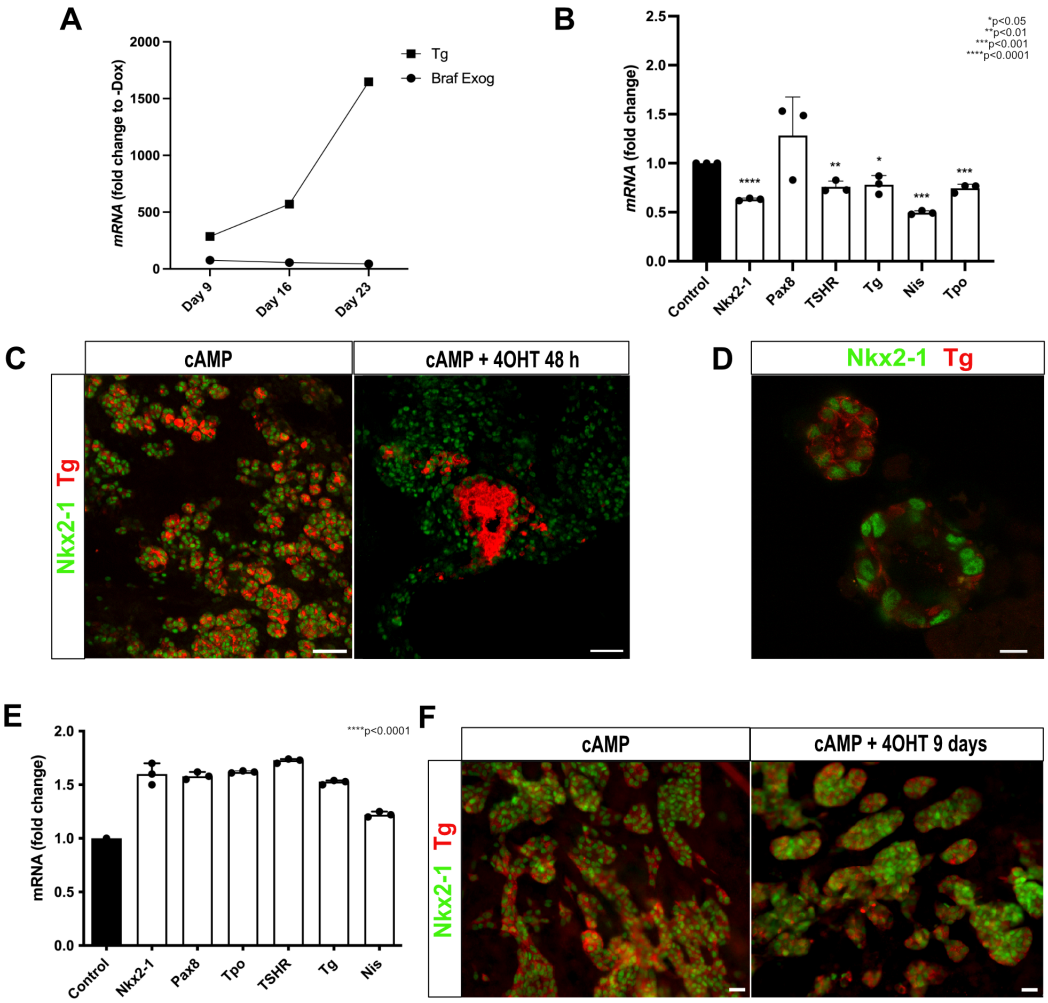

969

970 **Figure S3. 4OHT treatment rapidly induces Braf-carcinogenic changes in gene**
971 **expression and follicular organization.** Tg and Braf exogenous expression levels at day
972 9, 16, and 23 of thyroid differentiation protocol (A). Induction of Braf^{V637E} for 8 hours
973 promotes the downregulation of main thyroid genes (B). Nkx2-1 and Tg immunostaining
974 shows that under BrafV637E activation (4OHT; 48 h) thyroid follicles present bigger size
975 heterogeneous distribution of Tg compared to the control (C). Remaining follicular-like
976 structures after Braf^{V637E} activation (4OHT; 48 h) (D). mRNA expression of mESC-
977 Nkx2-1-Pax8_bTg-eGFP derived follicles treated for 9 days with 4OHT (E). Nkx2-1 and
978 Tg co-staining demonstrate that 4OHT treatment do not affect thyroid organization (F).
979 Scale bars, 50 µm (C), 20 µm (F) and 10 µm (D).

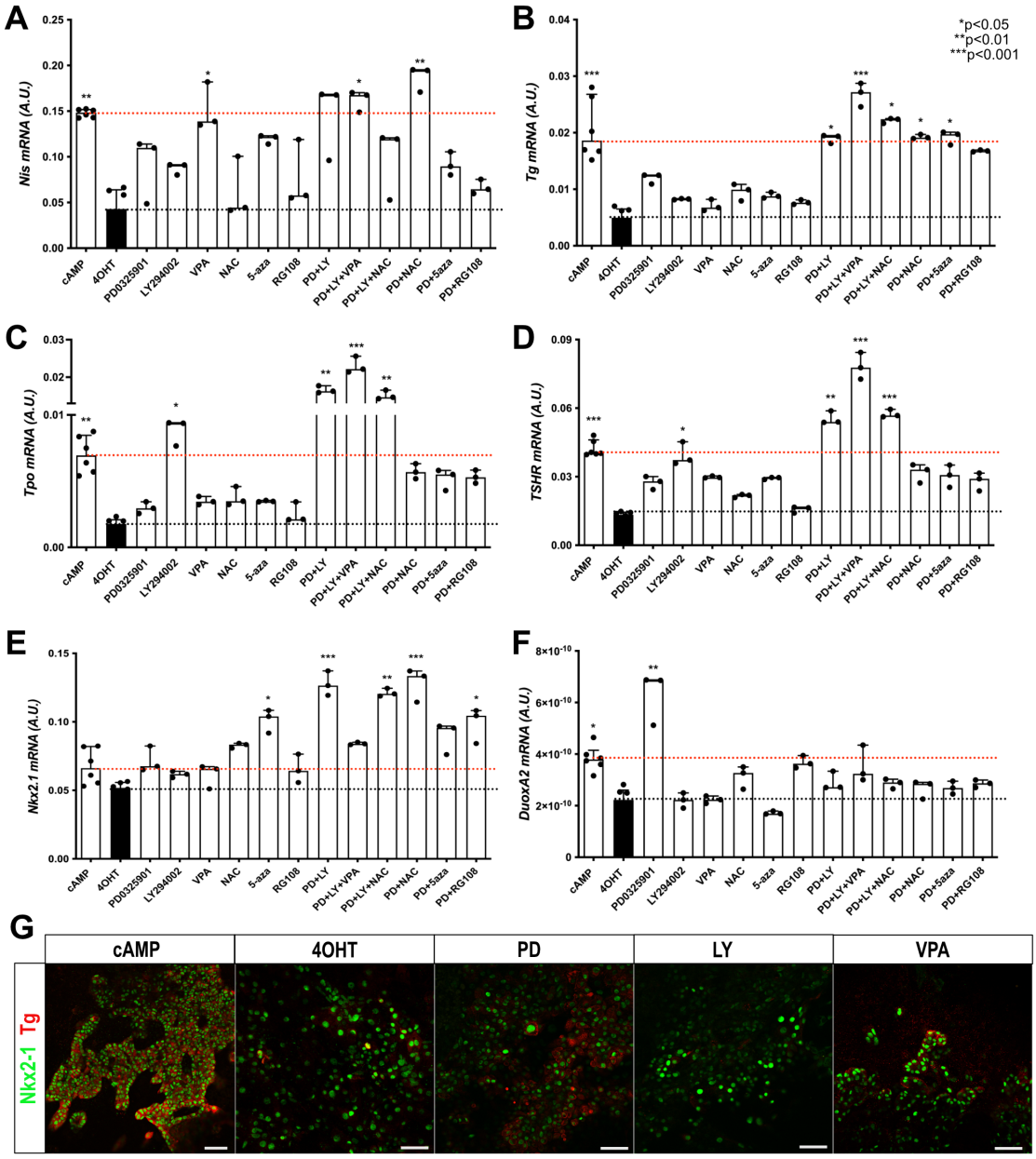

Figure S4. Effect of distinct classes of inhibitors on thyroid markers. Gene expression levels of *Nis* (A), *Tg* (B), *Tpo* (C), *TSHR* (D), *Nkx2.1* (E) *and Duox2A* (F) among normal thyroid organoids, Braf^{V637E}-expressing (4OHT) and treated with distinct inhibitor (4OHT+inhib). Significance is compared to 4OHT condition. Nkx2-1 and Tg co-staining shows that isolated PD0325901, LY294002 and VPA treatments are insufficient to revert the inhibitory effect of Braf^{V637E} activation on Tg expression and thyroid follicular organization. Scale bar, 50 µm.

989 **Supplementary tables**

990

991 **Supplementary Table 1.** Antibodies information.

Primary antibodies						
Protein Target	***Provider***	***Catalog number***	***Host Species***	***Dilution Flow Cyt.***	***Dilution IF***	***Dilution WB***
AFP	Santa Cruz	sc-8108	Goat		1:100	
β-III Tubulin	Eurogentec	MMS-435P-200	Mouse		1:1,000	
αSMA	Abcam	ab32575	Rabbit		1:1,000	
Nkx2-1	Abcam	ab76013	Rabbit	1 :100	1:500	
PAX8	Cell Signaling	59019	Rabbit		1:500	
Tg	Dako	A0251	Rabbit		1:2,000	
Tg	Abcam	Ab187378	Mouse		1:250	
Nis	Gift from N. Carrasco		Rabbit		1:1,000	
TG-I	Gift from C. Ris-Stalpers		Mouse		1:250	
E-cadherin	BD	610181	Mouse		1:1,000	
ZO-1	Invitrogen	339100	Mouse		1:500	
Hoechst	Invitrogen	33342			1:1,000	
p-ERK	Cell Signaling	4370	Rabbit			1:1,000
β-Actin	Cell Signaling	3700	Mouse			1:1,000
Secondary antibodies						
Cy3-conjugated	Jackson Immunoresearch	715-165-150	Donkey anti-mouse IgG		1:500	
Cy3-conjugated	Jackson Immunoresearch	711-165-152	Donkey anti-rabbit IgG		1:500	

Cy3-conjugated	Jackson Immunoresearch	705-165-147	Donkey anti-goat IgG		1:500	
Alexa fluor 488-conjugated	Jackson Immunoresearch	715-545-150	Donkey anti-mouse IgG		1:500	
Alexa fluor 647-conjugated	Jackson Immunoresearch	715-605-150	Donkey anti-mouse IgG		1:500	
Alexa fluor 647-conjugated	Jackson Immunoresearch	711-605-152	Donkey anti-rabbit IgG	1:300	1:500	
Anti-rabbit IgG, HRP-linked	Cell Signaling	7074				1:1,000
Anti-mouse IgG, HRP-linked	Cell Signaling	7076				1:1,000

992

993 **Supplementary Table 2.** List of primers used for RT-qPCR analysis.

Gene	**Primer Forward**	**Primer Reverse**
β2m-Globulin	GCTTCAGTCGTCAGCATGG	CAGTTCAGTATGTTCGGCTTCC
Nkx2-1 exog.	GGCGCCATGTCTTGTTCT	ACACCGGCCTTATTCCAAG
Nkx2-1	GGCGCCATGTCTTGTTCT	GGGCTCAAGCGCATCTCA
Pax8	CAGCCTGCTGAGTTCTCCAT	CTGTCTCAGGCCAAGTCCTC
Foxe1	GGCGGCATCTACAAGTTCAT	GGATCTTGAGGAAGCAGTCG
Tg	GTCCAATGCCAAAATGATGGTC	GAGAGCATCGGTGCTGTTAAT
Nis/Slc5a5	AGCTGCCAACACTTCCAGAG	GATGAGAGCACCACAAAGCA
Tshr	GTCTGCCCAATATTTCCAGGATCTA	GCTCTGTCAAGGCATCAGGGT
Tpo	ACAGTCACAGTTCTCCACGGATG	ATCTCTATTGTTGCACGCCCC
Braf exog.	GCTTGTGCTTCTCCGAAAAC	AAGGCCAGGCTGTTCTTCTT
Dio1	ATGGCCAGGAACCCCCG	GCCTGCTGCCTTGAATGAAA
Dio2	TTCTCCAACTGCCTCTTCCTG	CCCATCAGCGGTCTTCTCC
Gal3	TTGAAGCTGACCACTTCAAGGTT	AGGTTCTTCATCCGATGGTTGT
Fn1	AATCACAGTAGTTGCGGCAGGAGA	TCTGTCCCAGGCAGGAGATTTGTT

994

995 **Supplementary Table 3.** Gene list used for thyroid differentiation (TDS and eTDS) and

996 ERK scores calculation.

	TDS	eTDS	ERK score
Included	DIO1 DIO2 DUOX1 DUOX2 FOXE1 GLIS3 NKX2-1 PAX8 SLC26A4 SLC5A5 SLC5A8 TG THRA THRB TPO TSHR	BCL2 CDH16 CLCNKB DLG2 DPP6 FAM167A FHL1 FLRT1 GPM6A GRIN2C HGD KIT LMOD1 LRP2 MATN2 MPPED2 PKHD1L1 PLA2R1 SLC26A7 SLC4A4 SORBS2 STXBP5L TFCP2L1 TFF3 TPPP WSCD2 ZMAT4	ARID5A B4GALT6 BRIX1 BYSL CCND1 CD3EAP CHSY1 DDX21 DUSP4 DUSP6 EGR1 ELOVL6 ETV1 ETV4 ETV5 FOS FOSL1 GEMIN4 GTF2A1L GNL3 GPR3 GTPBP4 HMGA2 HYDIN IER3 KIR3DL2 LIF MAFF MAP2K3 MYC NOP16 PHLDA2 PLK3 POLR1C POLR3G PPAN PPAT PYCRL RRS1 SEMA6A SH2B3 SLC1A5 SLC4A7 SPRED2 SPRY2 SPRY4 TNC TNFRSF12A TSR1 WDR3 YRDC
Missing		LOC286002 MT1G	CXCL8

997